BOLT BERANEK AND NEWMAN INC

CONSULTING • DEVELOPMENT • RESEARCH

Report No. 3225

DETECTION PERFORMANCE OF AN OPERATOR USING LOFAR (U)

Magnus Moll

April 1976

ONR Contract No. N00014-71-C-0303
Task No. NR 274-236
BBN Job No. 10117

Submitted to:

Naval Analysis Programs Inc.
Office of Naval Research
Arlington, Virginia 22209

Attention: Mr. James G. Smith
Code 431

Submitted by:

Bolt Beranek and Newman Inc.
1701 North Fort Myer Drive
Arlington, Virginia 22209

Unclassified

SECURITY CLASSIFICATION OF THIS PAGE (When Data Entered)

REPORT DOCUMENTATION PAGE		READ INSTRUCTIONS BEFORE COMPLETING FORM
1. REPORT NUMBER	2. GOVT ACCESSION NO.	3. RECIPIENT'S CATALOG NUMBER
4. TITLE (and Subtitle) Detection Performance of an Operator Using Lofar (U)		5. TYPE OF REPORT & PERIOD COVERED Technical Report 6. PERFORMING ORG. REPORT NUMBER BBN Report No. 3225
7. AUTHOR(S) Magnus Moll		8. CONTRACT OR GRANT NUMBER(S) N00014-71-C-0303
9. PERFORMING ORGANIZATION NAME AND ADDRESS Bolt Beranek and Newman Inc. 1701 North Fort Myer Drive Arlington, VA 22209		10. PROGRAM ELEMENT PROJECT TASK AREA & WORK UNIT NUMBERS 65152N RTW31 NR 274-236
11. CONTROLLING OFFICE NAME AND ADDRESS Naval Analysis Programs (Code 431) Office of Naval Research Arlington, VA 22217		12. REPORT DATE April 1976 13. NUMBER OF PAGES 64
14. MONITORING AGENCY NAME & ADDRESS (if different from Controlling Office) N/A		15. SECURITY CLASS. (of this report) UNCLASSIFIED 15a. DECLASSIFICATION/DOWNGRADING SCHEDULE N/A

16. DISTRIBUTION STATEMENT (of this Report)

"Approved for public release; distribution unlimited."

17. DISTRIBUTION STATEMENT (of the abstract entered in Block 20, if different from Report)

N/A

18. SUPPLEMENTARY NOTES

19. KEY WORDS (Continue on reverse side if necessary and identify by block number)

Lofar Processing
Visual Signal Processing
Sonar Display Model
Sonar Operator Performance

20. ABSTRACT (Continue on reverse side if necessary and identify by block number)

Predicting the performance of a sonar system that incorporates Lofar processing requires quantitative information about the detection performance of the Lofar. If performance data regarding a particular model is not immediately available; it would be useful to have a means for predicting its performance given the processing and display parameters. A means for doing this is developed in this report. The results can

DD FORM 1 JAN 73 1473 EDITION OF 1 NOV 65 IS OBSOLETE

Unclassified

SECURITY CLASSIFICATION OF THIS PAGE (When Data Entered)

20. (cont'd)

also serve as a display design tool and as a means for determining ways of utilizing equipment more effectively.

The approach is based on information about the human visual system acquired by many researchers of diverse disciplines. This information is employed to formulate a processing analog whose detection performance is analyzed by statistical methods.

A pair of formulas is derived: one for the detection parameter from which the probability of detection can be calculated; and another for the signal-to-noise ratio required for a specified probability of detection. The results, which apply to a fully-alerted operator, depend on both display and viewing parameters. Although the formulas apply to a single look or eye fixation, the predictions made assuming nominal viewing parameters show very good agreement with the results of laboratory experiments in which neither the viewing parameters nor the number of looks were constrained.

Distribution List for

"Detection Performance of an Operator

Using Lofar"

	No. of Copies
Advanced Research Projects Agency Department of Defense Washington D.C. 20301 (Technical Library)	1
Defense Documentation Center Cameron Station Alexandria, VA 22314	12
Office of Naval Research Department of the Navy Arlington, VA 22217	
(Code 431)	2
(Code 455)	1
(Code 440)	1
(Code 200)	1
Commander Submarine Development Group Two Box 70, Naval Submarine Base New London, CT 06342	1
Applied Physics Laboratory Johns Hopkins University 8621 Georgia Avenue Silver Spring, MD 20910 (Mr. C. West)	1
Institute for Defense Analyses 400 Army Navy Drive Arlington, VA 22202	1
The Rand Corporation 1700 Main Street Santa Monica, CA 90401	1
General Research Corporation Westgate Industrial Park McLean, VA 22101	1

	No. of Copies
Naval Warfare Research Center Stanford Research Institute Menlo Park, CA 94025	1
General Dynamics Corporation Electric Boat Division Groton, CT 06340 (Mr. T. Downie)	1
U. S. Army Research Institute for the Behavioral and Social Sciences 1300 Wilson Boulevard Arlington, VA 22209 (Mr. Cecil D. Johnson)	1
Center for Naval Analyses 1400 Wilson Boulevard Arlington, VA 22209 (Library) (Dr. R. Beatty)	1 1
Naval Academy Annapolis, MD 21402 (Library)	1
Naval Postgraduate School Monterey, CA 93940 (Technical Library)	1
Naval War College Newport, RI 02840 (Technical Library)	1
Naval Air Development Center Johnsville Warminster, PA 18974	1
Naval Ship Research & Development Center Bethesda, MD 20034	1
Naval Undersea Center (Code 14) San Diego, CA 92132	1
Newport Laboratory Navy Underwater Systems Center Newport, RI 02840	1

	No. of Copies
Naval Ordnance Laboratory Silver Spring, MD 20910 (Technical Library)	1
Naval Research Laboratory Washington, D.C. 20390 (Code 2029)	2
(Technical Information Division)	6
Naval Weapons Laboratory (Code KCU) Dahlgren, VA 22448	1

Report No. 3225

DETECTION PERFORMANCE OF AN OPERATOR USING LOFAR (U)

Magnus Moll

April 1976

ONR Contract No. N00014-71-C-0303
Task No. NR 274-236
BBN Job No. 10117

Submitted to:

Naval Analysis Programs Inc.
Office of Naval Research
Arlington, Virginia 22209

Attention: Mr. James G. Smith
Code 431

Submitted by:

Bolt Beranek and Newman Inc.
1701 North Fort Myer Drive
Arlington, Virginia 22209

TABLE OF CONTENTS

LIST OF ILLUSTRATIONS

1.0 SUMMARY

Predicting the performance of a sonar system that incorporates lofar processing requires quantitative information about the detection performance of the lofar. If such information is not immediately available for a particular model, it would be useful to have a means for predicting its performance given the processing and display parameters. A means for doing this is developed in this report. The results would also serve as a display design tool and as a means for determining ways to utilize equipment more effectively.

Lofar equipment permits a sonar operator to detect a narrowband signal in a noise background. The equipment consists of a frequency analyzer and a two-dimensional display that is intensity-modulated (or reflectance-modulated in the case of electrosensitive paper recorders). In essence, the display presents a time history of the frequency distribution of the input energy. A steady narrowband signal appears as a line of different intensity from the background.

The performance that can be achieved with lofar equipment depends heavily on the performance of the human visual processing system and on how well the display format is matched to it. This system has been the subject of study for many decades by many researchers of diverse disciplines. The body of research found to be relevant to this problem pertains to the subject of receptive fields. Some of this research is reviewed in Section 2.0 of this report. In addition, psychophysical data were found and employed to characterize the type of receptive field whose structure is appropriate for the detection of elongated signal traces.

Based on the characteristics of that type of receptive field, the detection performance was derived by the methods of statistical detection theory. The analysis (Section 3.0) consists of four major parts:

1. Derivation of selected statistical measures of the lofar display markings.

2. Description of the retinal image of the display surface pattern.

3. Derivation of selected statistical measures of the response of the receptive field to the light producing the retinal image.

4. Calculation of the detection performance from the derived response measures.

The major result of the derivation is a pair of simple formulas: One (80) for the detection parameter from which the probability of detection can be calculated; and another (81) for the signal-to-noise ratio required for a specified probability of detection. (Ten times the logarithm [to the base 10] of this ratio is the recognition differential.)

The results, which apply to a fully-alerted operator, depend on two sets of parameters:

1. Display Parameters

   - Length and width of the display surface
   - Number of frequency cells
   - Number of statistically independent time samples

2. Viewing Parameters

- Angle and distance

Application of the results to an example with representative parameter values predicts the following performance characteristics:

1. Performance improves with record length, but at a diminishing rate.

2. Performance improves if the viewing angle is decreased.

3. Performance improves with the width of a frequency cell on the display, but only to the point where the cell width matches the width of the receptive field.

4. A modest advantage can be obtained by compressing the display in the time dimension. The advantage obtained depends on signal duration and viewing angle.

Although the equations apply to a single look or eye fixation, the predictions made assuming nominal viewing parameters show very good agreement with the available results of laboratory experiments in which neither the viewing parameters nor the number of looks was constrained. In particular, the experiments confirm conclusions 1, 2, and 4 above. Since the frequency cell width on the display was constant through the experiments, they did not provide a basis for evaluating prediction 3.

2.0 VISUAL PROCESSING

The visual processing systems of humans, as well as those of other higher-order mammals, are highly complex, consisting of millions of functional parts. These systems have been the subject of studies spanning decades by scientists from several disciplines, such as psychology and neurophysiology. The discussion of this section is based primarily on the work of neurophysiologists. However, the crucial visual parameters required for the performance analysis were derived from the results of psychophysical experiments, in which subjects communicate their responses to physical stimuli.

2.1 General Description

Figure 2.1 shows the principal components of the visual system. Each eye includes optical components, such as a lens, and a retina which includes not only millions of light sensitive receptors called rods and cones but millions of other cells which process the outputs of the receptors. The processed outputs are transmitted via neurons comprising the pair of optic nerves to the lateral geniculate for further processing, and then to the visual cortex for yet further processing.

The optical elements of the eye produce an image of the field of view on the mosaic of photosensitive receptors of the retina. Even when the eye is focused on a point in the field of view, the image of that point is spread over an area that includes several receptors; and it has been concluded that the resolving capability of the system is not limited by the size and density of the receptors. Even though the image of a large object is properly focused in the central area of the retina (the fovea), it may not be exactly focused in other areas; and these refractive errors tend to increase with distance from the fovea. However, the degradation is gradual,

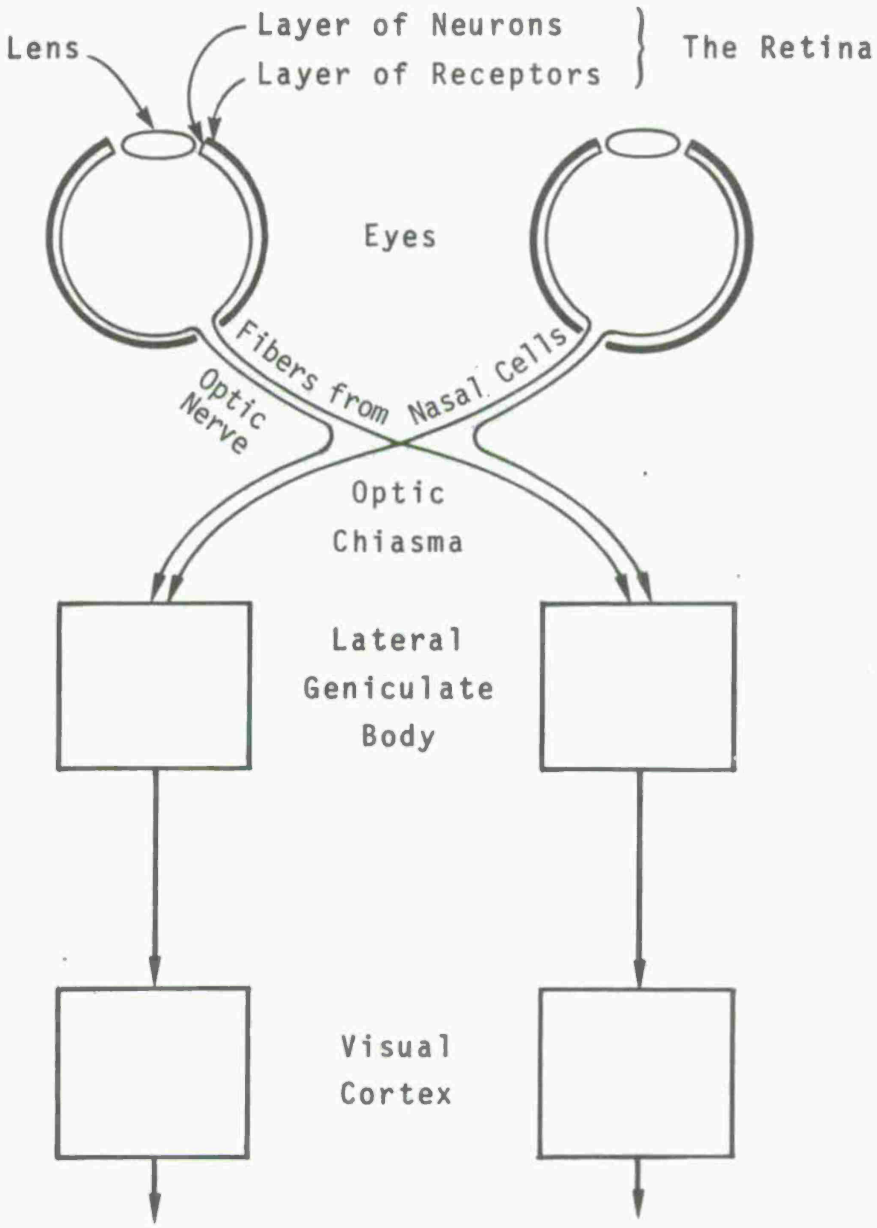

FIGURE 2.1 Representation of the Visual System.

and for images of the size that will be considered, the refractive errors will be assumed to be negligible. Furthermore, as will be discussed later, the functional units of the retina increase in size with displacement from the fovea so that the refractive errors are even less significant.

The retina includes a mosaic of photosensitive receptors, the rods and cones. The rods function at low (scotopic) light intensities, whereas the cones function at medium to high (photopic) intensities. There are many more rods (roughly 100 million) than cones (almost 10 million) in the retina. The density of cones is highest in the center of the fovea, and the density decreases rapidly with displacement from the center of the fovea, where visual acuity is greatest under photopic conditions. When a person is "looking" at an object, at least part of the image of that object falls on the fovea. The image of a sonar display viewed at normal distances will cover more than the foveal area, so the characteristics of peripheral vision are important to detection performance.

In dealing with objects and their images, it is convenient to specify their extent in terms of the visual angles they subtend. Angular measures are also employed to specify points on the retina. The meridian angle of a point is the angle between a vertical plane passing through the center of the fovea and the center of the lens and another plane that passes through those points and the point on the retina. The peripheral angle is the angle between the line that passes through the center of the lens and the center of the fovea, and a line that passes through the center of the lens and the point on the retina.

Typically, lofar displays and bearing-time recorders are viewed under photopic conditions; therefore, the cones and the processing of their responses is of primary interest. Based on counts by Osterberg, the density of cones (number per minute^2) along the temporal meridian is

$$p(\varepsilon) = 5.32 \exp(-1.88\varepsilon) + 1.24 \exp(-0.150\varepsilon) \quad (1)$$

where ε is the peripheral angle in degrees.[1] The first term accounts for the heightened density of cones in the foveal region. The contribution of this term is practically negligible above 2½ degrees.

The population of cones can be divided into three groups according to the dependence of their response on the frequency of the incident light. The response of each group peaks at a different frequency. The differences in spectral response is the basis for color discrimination under photopic conditions. Subsequent discussions in this report will not concern color discrimination.

The inner portion of the retina consists of layers of transparent cells that transfer and/or operate on the electrical impulses produced by the rods and cones. One important function is performed at the synapses, areas in which neural cells are contiguous. At an excitatory synapse, the excitation of one cell causes an excitation of another cell, while at an inhibitory synapse, the excitation of one cell reduces or inhibits the

---

[1]Derived from Equation (1) of D.H. Kelly, "Effects of the Cone-Cell Distribution on Pattern Detection Experiments," *Journal of the Optical Society of America*, (Vol. 64, No. 11) Nov. 1974, pp 1523-1525.

activity in another. Another important function is performed by the ganglion cells, that of collecting (or summing) the impulses received from multiple sensors. Each ganglion is connected to a single fiber in the optic nerve, which contains about 1 million neural fibers. Since the total number of receptors is much greater than the number of fibers, it is clear that if all of the sensors are employed, that some form of convergence, such as summation, must take place.

If a retina were to be uniformly illuminated, it would be found that the responses observed at the ganglions would vary with the rate of change of illumination. This implies that there would be no response to constant illumination, which seems contrary to experience. However, even when the gaze is fixed, the eyes undergo small involuntary rotations or drifts, which result in the retina moving relative to the image of the field of view. Thus, a temporally stable image with spatial variations of illumination give rise to responses from the sensors that are being swept under the nonuniform portions of the image. The average drift rate is a few minutes of arc per second. Periodically, a very quick movement called a saccade occurs in the reverse direction of the net drift. The average size of a saccade is about ten minutes of arc.[2] Although these movements are larger than the resolution of foveal vision, we are not aware of them. We will return to this matter later in this section.

As indicated by Figure 2.1, the neural fibers from a single eye proceed to two separate areas of the lateral geniculate body, which in turn are coupled to two distinguishable

---

[2]For further discussion, see Chapter XIV of Cornsweet, Visual Perception. His Figure 14.16 is a convincing demonstration of the insensitivity of the visual system to small rates of change of illumination.

areas of the visual cortex. The intersection of the optic nerve and the retina contains no receptors, and hence constitutes a blind spot on the retina.

2.2 Receptive Fields

Systems of many kinds can be characterized according to their responses to sets of specific stimuli. This approach is of great value for investigating systems of great complexity such as the visual system.

By neurophysiological methods, it is possible to obtain a great deal of information about the visual systems of animals under laboratory conditions. By the use of extremely fine electrodes, it is possible to monitor the impulse activity of neural cells of anesthesized animals generated by specific visual stimuli. The receptive field of a neuron is defined as that portion of the retina (or the corresponding visual field) that produces a response in the neuron when stimulated by light.

Fairly extensive data about the receptive fields of cells in different parts of the cat's visual system have been obtained. Hubel and Kuffler[3] investigated the receptive fields of retinal ganglions and those of neurons in the lateral geniculate body. Subsequently, Hubel and Wiesel investigated the characteristics of the receptive fields of cells in the visual cortex.

Recordings were made from acutely prepared anesthesized cats. Stabilization of the eyes was achieved by means of a paralyzing drug, and pupils were dilated with atropine. The

---

[3]This work is summarized in D.H. Hubel, T.N. Wiesel, "Receptive Fields, Binocular Interaction, and Functional Architecture in the Cat's Visual Cortex", *Journal of Physiology*, (No. 160), 1962, pp 106-154.

animal faced a wide screen, and various patterns of white light were shown on the screen. Recordings were made in the light-adapted state.

The eyes usually diverged slightly, so that points on the screen at the center of vision of each eye were not necessarily superimposed, a condition that allowed mapping the field associated with each eye separately.

In the retina, the receptive fields of the ganglions were found to have circular outlines as indicated by Fig. 2.2A. Each field consisted of two definable areas: a central circular area, and a surrounding concentric ring. Two types of fields were found. In the "on"-center field, a light stimulus in the center area (in this case called excitatory) caused an increase of the frequency of response impulses. In the concentric outer area, in this case termed inhibitory, the stimulus either reduced the impulse frequency or terminated the impulses completely; and the cessation of the stimulus was marked by a temporary increase of pulse frequency. For the "off"-center field, the positions of the excitatory and inhibitory areas were reversed. The numbers of each type of field observed were about equal. In either type of field, if the two areas are stimulated simultaneously, they react antagonistically and produce weaker responses than when the areas were excited separately. The size of the fields were found to increase with peripheral angle. Similar fields were found for the cells of the lateral geniculate body, which is further along the visual pathway.

Hubel and Weisel investigated the receptive fields in the cat cortex, further down the pathway. With the exception

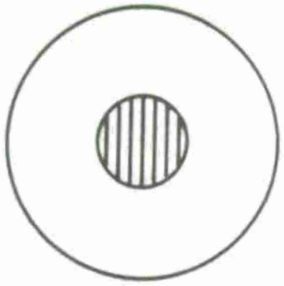

Circular (associated with neurons in the retina, optic nerve and lateral geniculate body)

A.

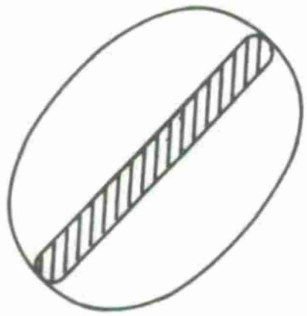

Excitatory center

B.

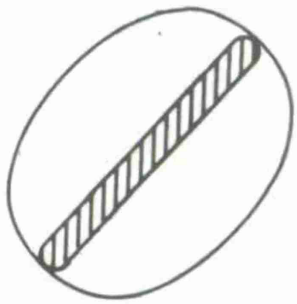

Inhibitory center

C.

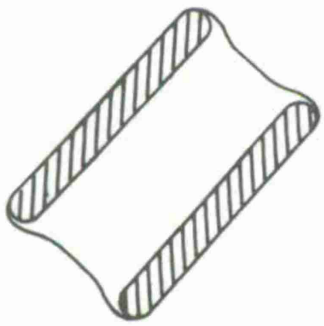

D.

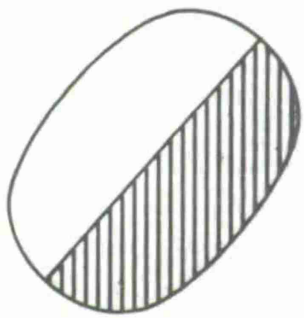

E.

FIGURE 2.2 Area Outline of Simple Receptive Fields.

of the fields of the incoming fibers from the lateral geniculate body, they found no circular receptive fields of the type observable in the retinal ganglions or in the cells of the lateral geniculate body.

The fields they observed were classified in two categories, simple or complex. Except for their shapes, the simple cortical fields were similar to the fields of the retina and the lateral geniculate body in that (1) they embraced distinct excitatory and inhibitory areas; (2) there was summation within each area; (3) responses of the two areas were antagonistic; and (4) the response to an arbitrarily shaped, fixed or moving stimulus can be predicted from the configuration of the excitatory and inhibitory areas. Complex fields do not have the properties listed above.

Figure 2.2 B-E illustrates the boundaries of areas of simple fields found in the cat cortex. All are characterized by having straight-line boundaries between excitatory and inhibitory regions. The orientation of a field is defined to be the orientation of its straight-line boundaries. The crosshatched areas could be either excitatory or inhibitory, and either arrangement appears to be equally likely. In Figure 2.2 A-D the crosshatched areas are much smaller than the remaining areas.

Since for simple fields there is summation within an area, the optimum stimulus for fields of the type in Figs. B and C would be a rectangular bar of light or dark for excitatory or inhibitory centers respectively. The orientation of the bar with respect to the center was found to be critical: orientation errors of 5 to 10^{o} greatly reduce the response or even abolish it. A stimulus of uniform light over an entire field produced either a very weak response or none at all, indicating that the magnitudes of the responses of the parts of the field were nearly or actually balanced.

Receptive fields not having the properties defining simple fields are termed complex. Hubel and Wiesel found many complex fields of diverse character. An example of special interest is depicted in Fig. 2.3. The overall extent of this field is $2\frac{1}{2}^{\circ}$ by 3°. The maximum response to a stationary stimulus was obtained by a bar of light $1/8^{\circ}$ wide extending across the field in the direction indicated by the dashed lines. The position of the bar was not critical, but its orientation was. As indicated by the lower portion of Fig. 2.3, the response to a pulse of light was the combination of both on and off responses. For complex fields, such mixed responses are not uncommon; this is in contrast to simple fields where the optimal stimulus provokes either on responses or off responses. The cell was found to respond strongly and continuously when the optimum stimulus was moved across the field at a steady rate, and for this field, the optimum rate of movement was about one degree per second. Continuous response could also be maintained by small to and fro movements of the stimulus.

As discussed previously, the normal involuntary eye movements cause the retina to drift slightly with respect to a stationary image. Consider a constant light bar stimulus of a specified orientation, size, and shape. We would expect to find a large population of fields of the type depicted by Fig. 2.2B that at least approximately match the specifications of the image. As the retina drifts under the image, several of these fields will produce transient responses in succession. In contrast, consider a complex field of the type discussed above encompassing the area of image excursion whose optimum stimulus approximately matches the specifications of the applied stimulus. As long as the stimulus is maintained and there is no gross eye

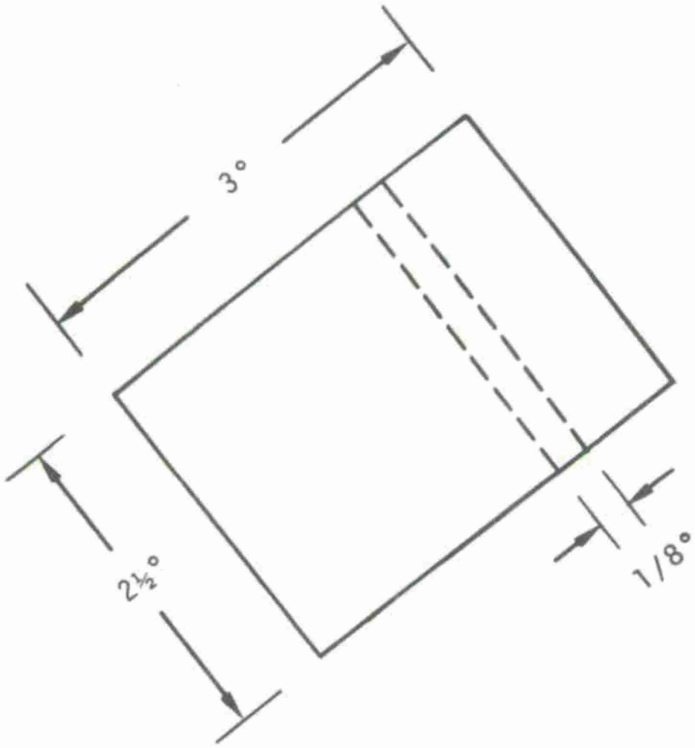

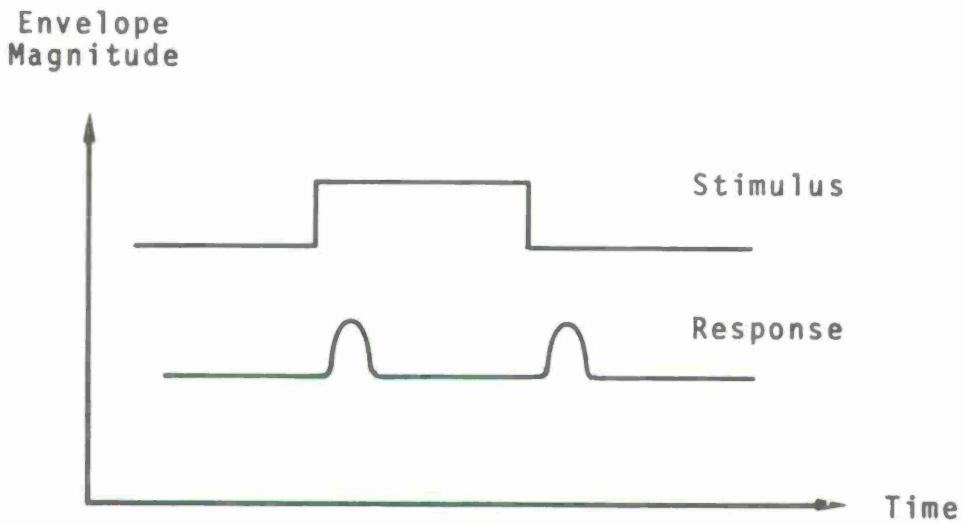

FIGURE 2.3 Pertaining to One Type of Complex Receptive Field.

movement, the output of such a cell would continuously be maintained, and would produce no sensation of drift.

The type of complex field discussed above, if present in the human visual system, would be expected to play an important role in the detection of elongated signal traces in a background of noise markings. Comparable data on the receptive fields of humans do not exist. However, there are data from psychophysical experiments (discussed in the next section) that can be employed if the pertinent hypothesis advanced by Hubel and Wiesel, op. cit., is accepted.

In essence that hypothesis states that a field of higher complexity is achieved by collecting the outputs of an appropriate set of fields of lower complexity.

Two related examples will serve as illustrations. A simple cortical field of Type B in Figure 2.2 could be synthesized from a set of overlapping geniculate fields (Type A) whose inner areas have diameters equal to the width of the inner area of the Type B field, and whose centers fall on the centerline of the B field.

A set of these Type B fields with the same size and orientation, with center overlapping and deployed with their edges along a line orthogonal to their axes, could be employed to synthesize the complex field described in previous paragraphs. To achieve the mixed temporal response, an equal distribution of on and off center fields would be required. This mode of synthesis raises a question. Suppose the optimum stimulus were projected on some area of the field? What happens if another bar of similar size and orientation but

displaced from the first is projected onto the field? If the separation were sufficient so that there were no inhabitory responses induced in the pair of simple fields whose centers coincided with the stimulus bars, then a response stronger than that from the first bar would be expected. If the separation were reduced so that the bars were just abutting, the response would be less than maximum because the (now) single stimulus does not have optimum width.

2.3 Receptive Field Data

To predict the capability of sonar operators of detecting elongated signal traces in a background of noise markings, it would be useful to have the following information available.

1. The presence or absence of complex fields of the type just described in the previous section in the human visual system.

2. Given the existence of such fields, their distribution over the retina; the overall size of these fields; the dimension and rates of movement for optimal stimulae; and finally the response function over the stimulus areas.

Due to the severity of the laboratory procedures required to obtain neurophysiological data, it is necessary to employ psychophysical experiments to infer the data. (Even if neurophysiological methods could be employed, it would be difficult to obtain all of the data.) With psychophysical experiments, it is difficult to deduce the desired field properties because the receptive fields are highly overlapped, and a single

stimulus may excite many of them. The final decision by the observer may be influenced by the outputs of at least several fields. Results could also be influenced by involuntary eye movements. However, if the durations of the stimuli are brief, enough, such effects are negligible.

A search of the literature has not revealed any psychophysical experiments directly pertaining to elongated receptive fields. However, two sets of experiments have been reviewed that provide data pertaining to circular receptive fields. Given the characteristics of circular fields, it should be possible to deduce the characteristics of an elongated field, given that the latter is synthesized from a set of the former (the Hubel-Wiesel hypothesis).

A set of experiments were conducted first by Westheimer,[4] and then by Enoch, Sunga, and Bachmann[5] with concentric circular light stimuli.

The inner portion of the stimulus was a small flashing disc of light, maintained at a fixed luminance level and area at a predetermined position in the visual field. The surrounding ring was a non-flashing area of illumination whose level was varied to determine the luminance level required to make the inner, flashing field appear and disappear. Conducting this procedure with different diameters of the surrounding ring generated data pertaining to the size of the receptive field areas.

---

[4]G. Westheimer, "Spatial Interaction in Human Cone Vision," *J. Physiol*, (1967), 190, pp. 139-154.

[5]Jay M. Enoch, R.N. Sunga, and E. Bachmann, "Static Perimetric Technique Believed to Test Receptive Field Properties I. Extension of Westheimer's Experiments on Spatial Interaction. *Am. J. Ophthalmology*, 70, No. 1, July 1970, pp. 113-126.

A typical set of results from Enoch, et alii, are shown by Figure 2.4. Here, each curve pertains to a different level of luminance of the flashing center disc. A curve is generated by selecting the size of the surrounding ring, and then determining the level required to extinguish the appearance of the flashing center. The descending portion of each curve has been termed the summation arm, and the ascending portion has been termed the inhibition arm. It is reasonable to expect that light falling in the inner area of the receptive field will raise the threshold for observing the flashing center. If the size of the surrounding ring is increased, but not beyond the summation area of the receptive field, then a lower level of light intensity will produce a given amount of light flux. However, if part of the surrounding ring falls on the inhibition area of a field, then the threshold for observing the flashing center light will decrease, and the intensity of the center ring would have to be increased to achieve masking of the flashing center.

For the three upper curves of Figure 2.4, the intrusion of the surrounding light ring into the area of inhibition is easily observed. At the lowest level, the inhibition is absent, or poorly developed.

As long as an increase in the area of the surrounding ring causes a significant change in threshold, the area of neural interaction has not been exceeded. This limiting area of neural interaction is regarded as an estimate of receptive field size. However, as seen from Figure 2.4 this value is subject to interpretation since the rate of change of threshold with ring area decreases with increasing area.

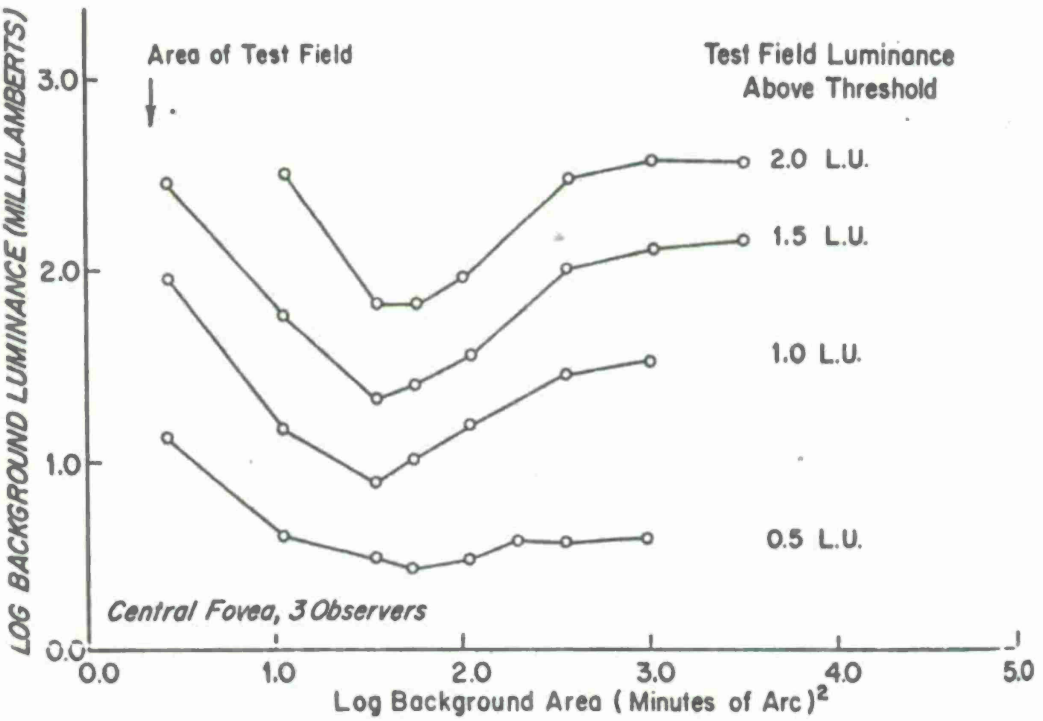

Source: Enoch, et alii, op. cit.. The log background luminance necessary to just make the flashing test field disappear (ascending threshold) determined for each of several different size backgrounds.

FIGURE 2.4 Masking Threshold Values.

Data were obtained with the flashing spot at different periperal angles (the data of Figure 2.4 pertain only to the foveal area). Figure 2.5 shows both ring areas corresponding to the minimum threshold and the limit of interaction obtained by Westheimer and by Enoch, et alii. For the minimum values, the agreement of the two sets of data is good. For the limit of interaction, the data are somewhat disparate, but this is not surprising in view of the discussion in the previous paragraph, and because the value may be dependent on overall illumination level.

For the diameter of the center area of a field, Westheimer's data are approximated by a line given by

$$d_s = 7 + |\varepsilon|/20 \quad , \text{arc minutes} \qquad (2)$$

where ε is the peripheral angle in arc minutes. For the outer diameter of the field, the average of the data of Westheimer and Enoch et alii is about three times that of the center area.

If it is assumed that a simple line detector is synthesized from a set of circular fields whose centers fall on the same straight line, the result would appear as shown in Figure 2.6 for a field centered on the fovea. The width of the center portion of the field is assumed to be

$$w_s = 7 + |\varepsilon|/20 \quad , \text{arc minutes} \qquad (3)$$

The width of the outer portion of the field is assumed to be three times that of the inner portion.

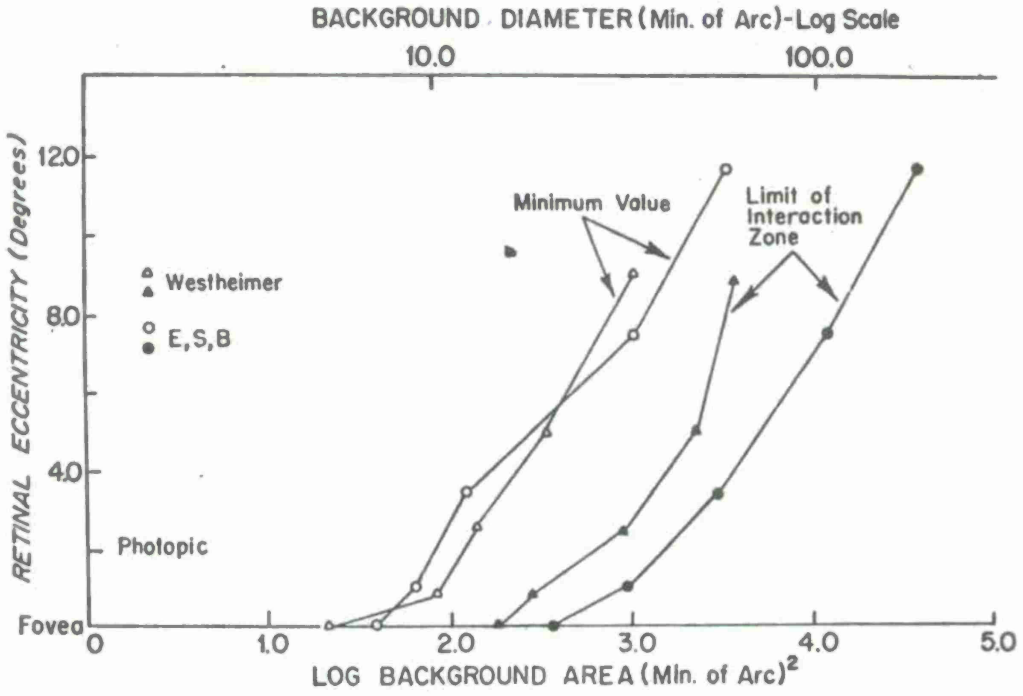

Source: Enoch, et alii, op. cit.. Derived dimensions of areas of neural interaction (photopic) are presented as a function of displacement from the point of fixation (ordinate). In addition, minima falling between the summation and inhibition arms of these functions are plotted.

FIGURE 2.5 Field Areas.

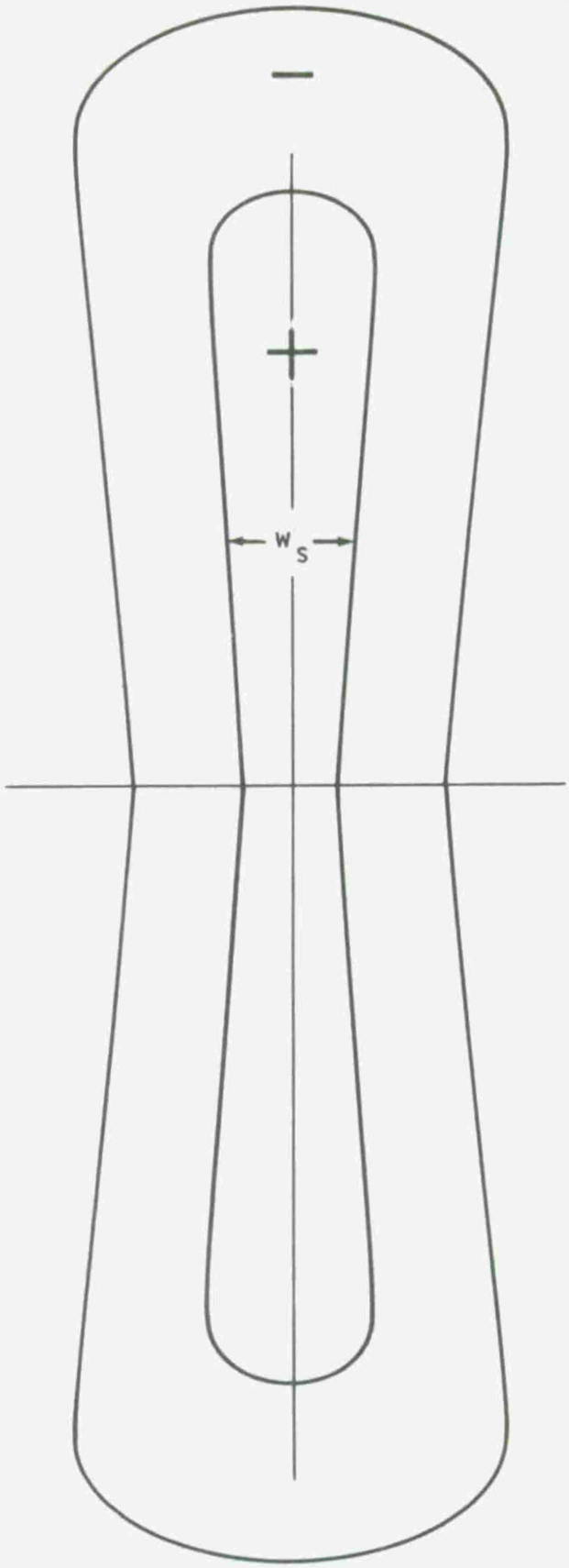

FIGURE 2.6 Representation of a Simple Line Detector.

The length of the field has not been specified. It is assumed that there are many fields of different lengths, and that one of these will match, or nearly match, the length of the signal trace.

3.0 LOFAR DETECTION PERFORMANCE

3.1 Introduction

Lofar equipment is designed to permit a sonar operator to detect the presence of a narrowband signal in a noise background. The equipment consists of a frequency analyzer and a recording display. In essence, the display presents a time history of the frequency distribution of the input energy. If the recording medium is electrosensitive paper, the reflectance varies inversely with signal intensity. If a cathode ray oscilliscope is employed, the luminance usually varies with the signal intensity. A steady narrowband signal appears as a line of different intensity from the background.

The objective of this analysis is to derive the probability of detecting a single narrowband signal by means of one of the line detector receptive fields. The elements involved are shown in Figure 3.1. The analysis consists of four major parts:

1. Derivation of certain statistical measures of the Lofar display markings in terms of the input voltage statistics.

2. Description of the retinal image of the marking pattern on the display surface.

3. Derivation of statistical measures of the response of a receptive field to the retinal image.

4. Calculation of the detection performance from the derived response measures.

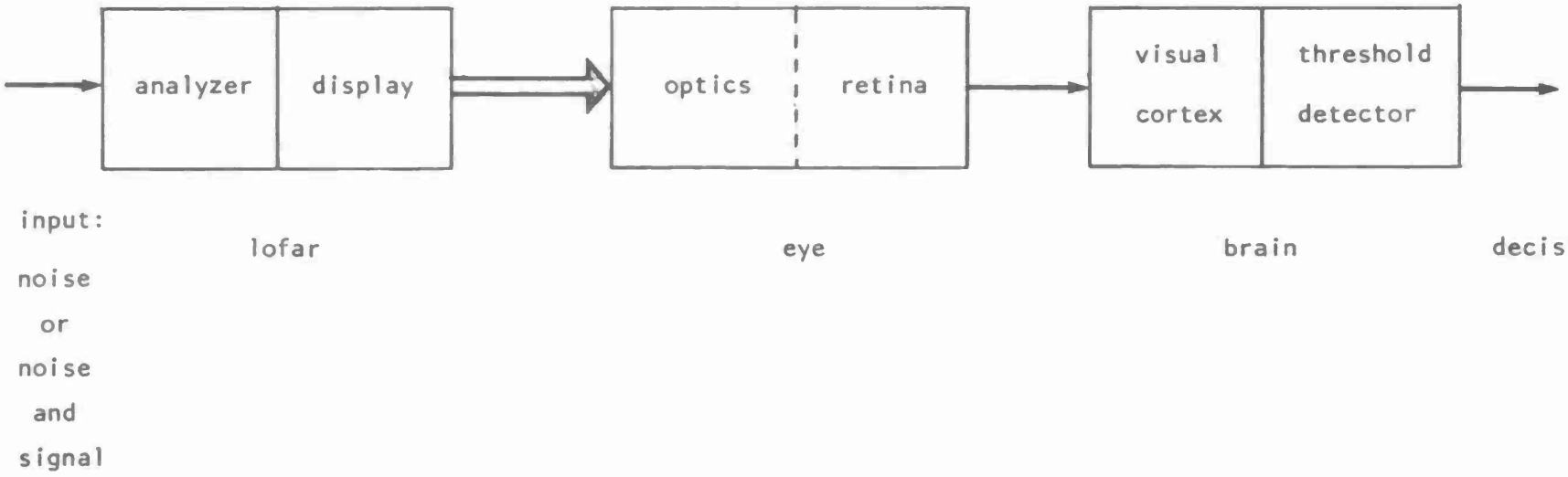

FIGURE 3.1 Elements of the Problem.

Implications of the calculations will be discussed and compared to the results of detection threshold measurements obtained by means of psychophysical experiments conducted in a laboratory.

3.2 Statistics of Display Markings

Lofar processing has been implemented with different circuit technologies, and the circuit details do influence the transfer characteristics. This subject has received considerable attention,[6] whereas the second stage, the visual processing, has been almost totally ignored. Since our emphasis is on the latter, a reasonably simple representation of the electronic circuits is chosen.

The circuit analog employed to represent the Lofar equipment is shown in Figure 3.2. The input, which could either be the output of a single hydrophone or a beamformer, is applied simultaneously to a bank of narrowband filters. For convenience, it is assumed that the bandpass functions are rectangular and contiguous. The output of each filter is squared and filtered to remove the high frequency components prior to sampling, which is performed at a rate numerically equal to the filter bandwidth (i.e., twice the half bandwidth). The sampled data are converted to digital form and are stored in a memory. These stored data are scanned at a rate required to refresh the display. Sample sets are advanced at the analog sampling rate, and the oldest samples are discarded.

---

[6] e.g., C. N. Pryor, "Calculation of the Minimum Detectable Signal for Practical Spectrum Analyzers," *Naval Ordnance Laboratory Technical Report 71-92*, August 1971.

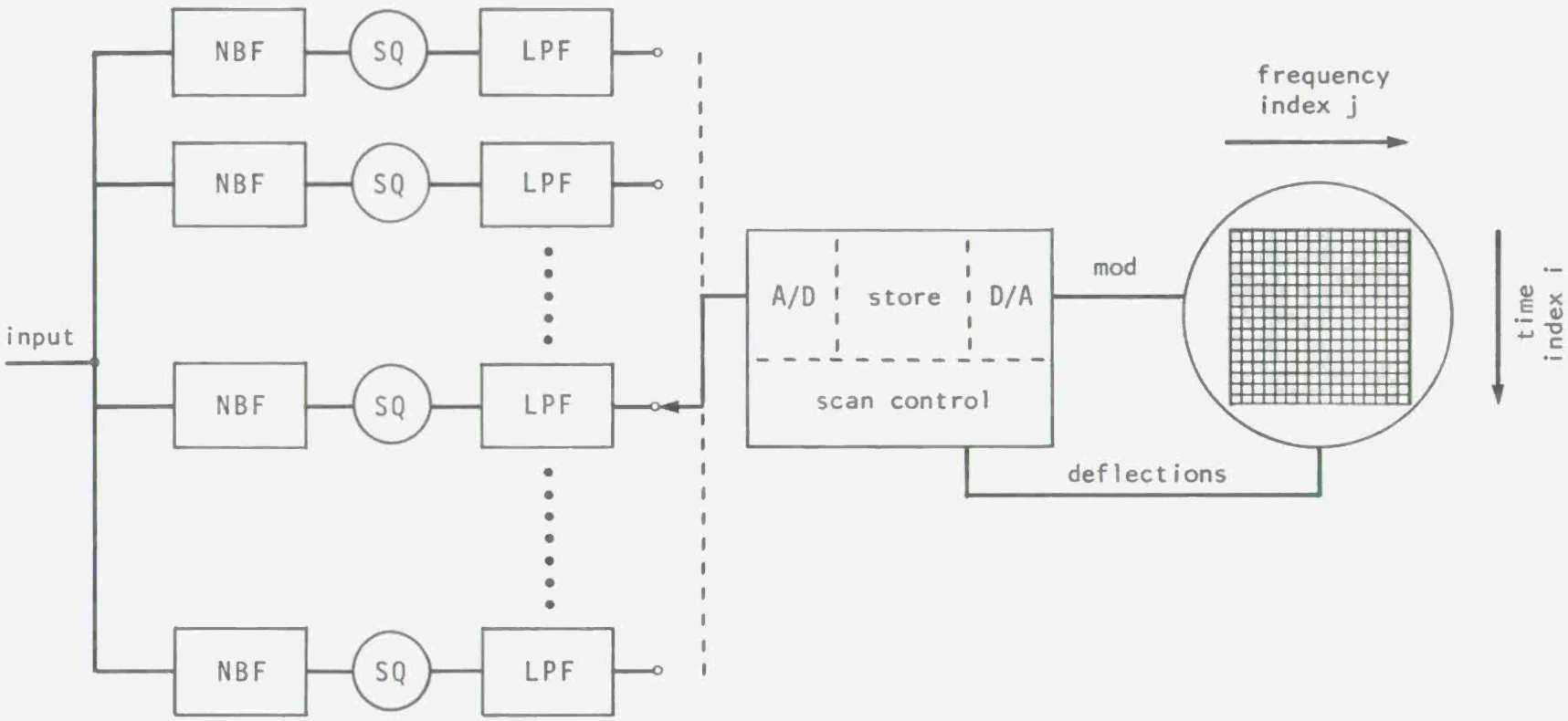

FIGURE 3.2 Lofar Analog.

The luminosity of a sample marking X_{ij} is assumed to be related to the sampled voltage V_{ij} by

$$X_{ij} = c + kV_{ij} \tag{4}$$

where c and k are constants
i is the index for the sampling time
j is the index for the frequency channel

The first and second (mixed) moments for the marking samples are, respectively

$$E(X_{ij}) = c + kE(V_{ij}) \tag{5}$$

$$E(X_{ij}\ X_{kl}) = c^2 + ck\left[E(V_{ij}) + E(V_{kl})\right] + k^2E(V_{ij}\ V_{kl}) \tag{6}$$

where E represents statistical expectation.

The output of the i^{th} narrowband filter can be represented as

$$U_j(t) = P_j(t) \cos 2\pi f_j t + Q_j(t) \sin 2\pi f_j t \tag{7}$$

If $U_j(t)$ is assumed to be a Gaussian process, then $P_j(t)$ and $Q_j(t)$ are Gaussian processes with the same autocovariance K(T). If $U_j(t)$ is squared and lowpass filtered, the result is

$$V_j(t) = (1/2)\ [P_j^2(t) + Q_j^2(t)] \tag{8}$$

The mean value of a sample of $V_j(t)$ is

$$E(V_{ij}) = P_{Nj} \tag{9}$$

where P_{Nj} is the power of the noise in channel j.

If a signal is present in channel n, then

$$E(V_{in}) = P_{Nn} + P_{Sn} \tag{10}$$

where P_{Sn} is the power of the signal in channel n

For the case of noise alone, the second moment function for $V_j(t)$ is

$$E[V_j(t)V_j(t + T)] = P_{Nj}^2 + K^2{}_j(T) \tag{11}$$

If the noise in the band has a uniform spectrum, then samples that are spaced by the reciprocal bandwidth are uncorrelated. Furthermore, if the bandpasses are non-overlapping but of the same bandwidth,

$$E[V_j(t)V_1(t + T)] = P_N^2 \tag{12}$$

Thus, for the output samples,

$$E(V_{ij}\ V_{kl}) = \begin{cases} P_N^2, & (i,j) \neq (k,l) \\ 2P_N^2, & (i,j) = (k,l) \end{cases} \tag{13}$$

The marking statistics derived from (5), (6), (9) (10), and (13) are

$$E(X_{ij}) = \begin{cases} c + kP_N \text{ , if } P_{Sj} = 0 \\ c + k(P_N + P_S) \text{ , if } P_{Sj} > 0 \end{cases} \quad (14)$$

$$E(X_{ij}\ X_{kl}) = \begin{cases} (c + kP_N)^2 \text{ , } (i,j) \neq (k,l) \\ (c + kP_N)^2 + (kP_N)^2 \text{ , } (i,j) = (k,l) \end{cases} \quad (15)$$

3.3 The Display Image

To calculate the response of a receptive field to the markings on a portion of the display, it is necessary to map the display image on that portion of the retina. Consider a region near a displayed line whose image would fall on the vertical meridian of the retina. The most convenient reference axis is the line which passes through the center of the fovea and the center of the lens. The point on that axis whose image is in focus on the retina is called the fixation point, and it is assumed that that point is the intersection of the axis with the display surface. The displacement of an image point falling on the vertical meridian is given by the angle ε shown in Figure 3.3, and the corresponding point on the display surface is a distance ℓ from the fixation point. The relationship between these quantities is found from the law of sines:

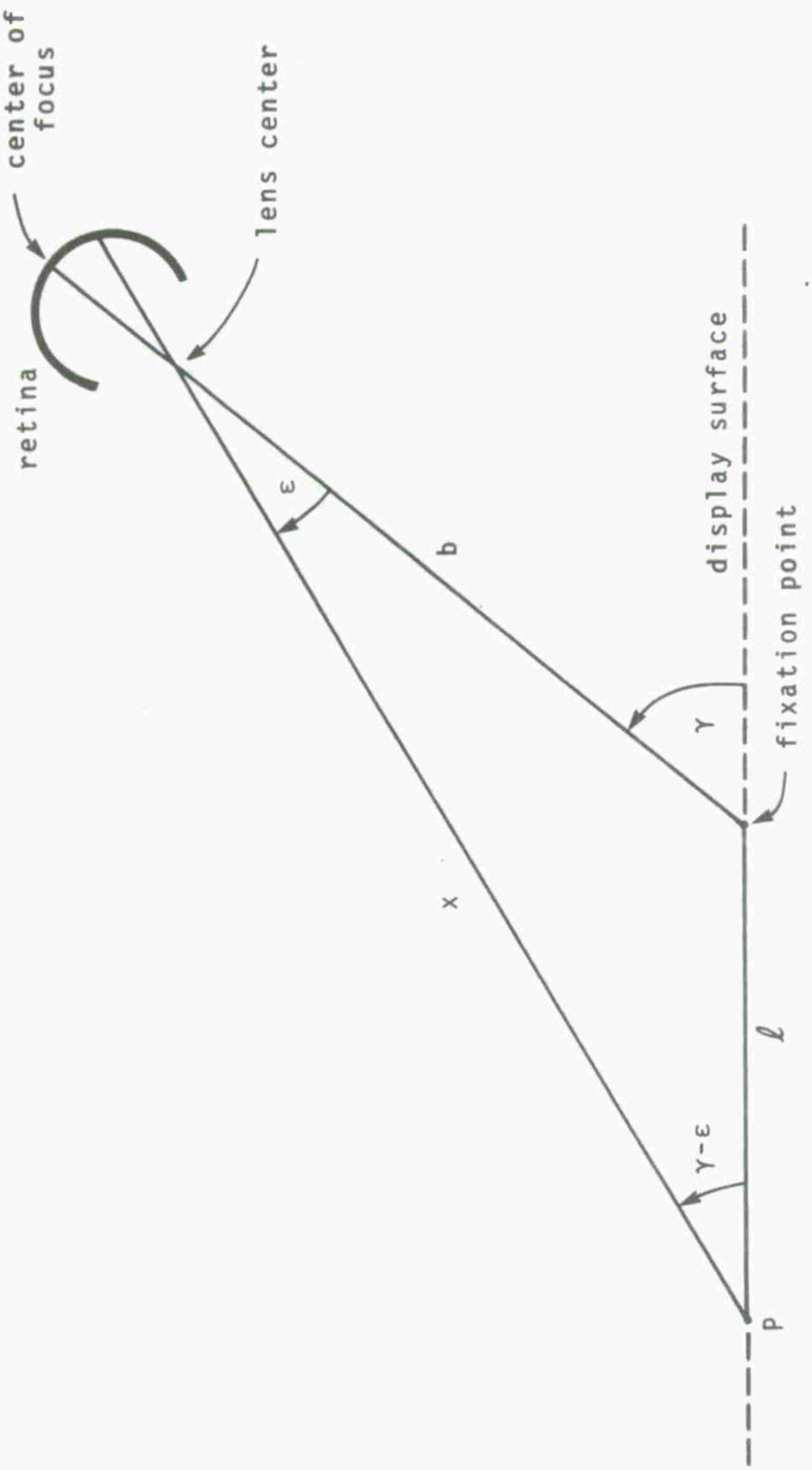

FIGURE 3.3 Viewing Geometry.

$$\frac{\ell}{\sin \varepsilon} = \frac{b}{\sin (\gamma - \varepsilon)} \tag{16}$$

where γ specifies the viewing angle
b specifies the viewing distance

Solving for ℓ and differentiating with respect to ε yields, after algebraic and trigonometric operations,

$$\frac{d\ell}{d\varepsilon} = \frac{b \sin \gamma}{\sin^2 (\gamma - \varepsilon)} \simeq \frac{\Delta\ell}{\Delta\varepsilon} \tag{17}$$

which relates the two differentials, and approximates the relationship between corresponding incremental quantities such as the space occupied by a mark. The length of a display mark in the time dimension is

$$\Delta\ell = h/t \tag{18}$$

where h is the height of the record in the time dimension
t is the number of marks in the time dimension.

The length of the mark image is found by substituting (18) in (17) and solving for $\Delta\varepsilon$. Conversion from radians to arc minutes gives

$$\ell_m = \frac{180 \cdot 60\ h \sin^2 (\gamma - \varepsilon)}{\pi t b \sin \gamma} \tag{19}$$

For cases in which the record is developed on electrosensitive paper of indefinite length, the length of a display mark in the time dimension is

$$\Delta\ell = n^{-1} = s/r \tag{20}$$

where n is the number of marks per inch
s is the speed at which the paper advances, in/min
r is the stylus sweep frequency, min^{-1}.

The width of a display mark in the frequency dimension is

$$\Delta w = w/c \tag{21}$$

where w is the width of the display
c is the number of frequency cells

The corresponding image width in arc minutes is

$$w_m = \frac{180 \cdot 60}{\pi} \cdot \frac{w/c}{x} \tag{22}$$

From Figure 3.3 and the law of sines we readily obtain

$$x = \frac{b \sin \gamma}{\sin (\gamma - \varepsilon)} \tag{23}$$

and substituting the result in (22) gives

$$w_m = \frac{180 \cdot 60\ w \sin (\gamma - \varepsilon)}{\pi c b \sin \gamma} \tag{24}$$

Finally, the angular coordinate associated with the point P of Figure 3.3 can be derived from (16). Multiplying its means and extremes gives

$$\ell \sin (\gamma - \varepsilon) = b \sin \varepsilon , \tag{25}$$

and expanding the left hand side gives

$$\ell(\sin \gamma \cos \varepsilon - \cos \gamma \sin \varepsilon) = b \sin \varepsilon \tag{26}$$

Rearranging (26) gives

$$\frac{\sin \varepsilon}{\cos \varepsilon} = \frac{\ell \sin \gamma}{b + \ell \cos \gamma} \tag{27}$$

Thus:

$$\varepsilon = \arctan \frac{\ell \sin \gamma}{b + \ell \cos \gamma} \tag{28}$$

The time period corresponding to a trace of length ℓ on recording paper is

$$T = \ell / s \text{ , seconds} \tag{29}$$

Solving for ℓ and substituting the result in (28) gives

$$\varepsilon = \arctan \frac{Ts \sin \gamma}{b + Ts \cos \gamma} \tag{30}$$

This relationship gives the peripheral angle associated with a record duration T for the specified viewing angle and distance.

The special case of an image centered on the retina is depicted by Figure 3.4, and it is desired to determine the peripheral angle. Applying the law of sines to the largest triangle gives

$$\frac{\sin 2\varepsilon}{h} = \frac{\sin (\gamma - \varepsilon)}{y} \tag{31}$$

and applying the same law to the triangle with sides b and y gives

$$\frac{\sin \gamma}{y} = \frac{\sin (\pi - \gamma - \varepsilon)}{b} = \frac{\sin (\gamma + \varepsilon)}{b} \tag{32}$$

Solving (32) for y and substituting the result in (31) gives

$$\frac{\sin 2\varepsilon}{h} = \frac{\sin (\gamma + \varepsilon) \sin (\gamma - \varepsilon)}{b \sin \gamma} \tag{33}$$

The solution of this equation is found to be

$$\tan \varepsilon = \frac{\tan \gamma}{h \cos \gamma} \left[\sqrt{b^2 + (h \cos \gamma)^2} - b \right] \tag{34}$$

3.4 Receptive Field Detection Performance

The signal detection performance of a receptive field will be predicted by deriving statistical measures of its response to the display image.

The type of field assumed to be operative for this task is the complex field of the type discussed in Section 2.2 and depicted by Figure 2.3. Such a field could produce a

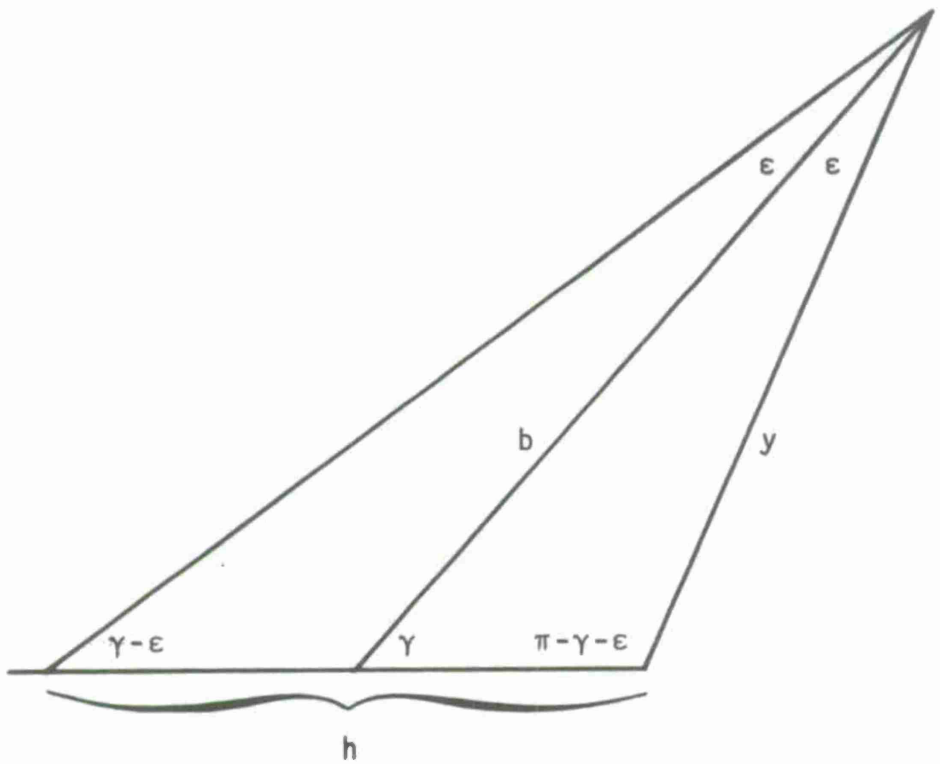

h: length of trace

FIGURE 3.4 Image Centered on Retina.

steady response to a fixed object despite the drift movement of the retina. However, to simplify the analysis, it will be assumed that the image is stationary on the retina, and that the operative field is of the simple type depicted by 2.7.

Response Function

If a single receptor responds in proportion to the intensity of the incident light, then the incremental response of the field to an incremental illuminated area can be expressed as

$$\Delta Y = \rho f \Delta A k' X \tag{35}$$

where ρ is the local density of cones

f is the fraction of cones employed in the receptive field times the sign of the response

ΔA is the incremental area

k' is a constant

X is the luminance of the object corresponding to the area of the retinal image.

The response of the receptive field to a set of markings can be written as

$$Y = k' \sum_i \int_{\alpha_i}^{\omega_i} du \sum_j \int_{\beta_j(u)}^{\psi_j(u)} dv \; \rho(u,v) f(u,v) X_{ij} \tag{36}$$

where u and v are the angular coordinates of a point on the retina

$\rho(u,v)$ is the cone density function

$f(u,v)$ is the field weighting function

X_{ij} is the luminance of mark ij

α_i and ω_i are the end points of the i^{th} time sample

$\psi_j(u)$ and $\beta_j(u)$ are the end points of the j^{th} frequency sample at u.

This formulation assumes that the field axis is aligned with the time dimension, and that the display surface is uniformly illuminated.

Noise Alone - Mean and Variance

By taking the expected value of (36) and by making use of (14) it is determined that the average of the field response to noise alone is

$$m_{YN} = E(Y)$$

$$= k'(c + kP_N)\sum_i \int_{\alpha_i}^{\omega_i} du \sum_j \int_{\beta_j(u)}^{\psi_j(u)} dv\ \rho(u,v)f(u,v) \qquad (37)$$

$$= k'(c + kP_N)\int_{\alpha}^{\omega} du \int_{\beta}^{\psi} dv\ \rho(u,v)f(u,v) \qquad (38)$$

Where α and ω mark the extent of the field in the time dimension
β and ψ mark the extent of the field in the frequency dimension.

The double integral is the response to uniform illumination of unit intensity. If it is assumed that the response of a uniformly illuminated cortical receptive field is zero, then the integral is zero and:

$$m_{YN} = 0 \tag{39}$$

for noise that is statistically uniform.

The square of the response is

$$Y^2 = (k')^2 \sum_i \int_{\alpha_i}^{\omega_i} du \sum_j \int_{\beta_j(u)}^{\psi_j(u)} dv \rho(u,v) f(u,v)$$

$$\times \sum_k \int_{\alpha_k}^{\omega_k} dw \sum_\ell \int_{\beta_\ell(w)}^{\psi_\ell(w)} dx \rho(w,x) f(w,x) X_{ij} X_{kl} \tag{40}$$

Since the mean response to noise alone is zero, the variance of the response is equal to its expected square. Taking the expected value of (39) and making use of (15) gives:

$$\sigma_Y^2 = (k')^2 (c + kP_N)^2 \sum_i \int_{\alpha_i}^{\omega_i} du \sum_j \int_{\beta_j(u)}^{\psi_j(u)} dv \rho(u,v) f(u,v)$$

$$\times \sum_{\substack{k \\ k \neq i}} \int_{\alpha_k}^{\omega_k} dw \sum_{\substack{\ell \\ \ell \neq j}} \int_{\beta_\ell(w)}^{\psi_\ell(w)} dx \rho(w,x) f(w,x)$$

(equation continued to next page)

$$+ \quad (k')^2 \left[(k + cP_N)^2 + (cP_N)^2 \right] \sum_i \sum_j \int_{\alpha_i}^{\omega_i} du \int_{\beta_j(u)}^{\phi_j(u)} dv \rho(u,v) f(u,v)$$

$$\times \int_{\alpha_i}^{\omega_i} dw \int_{\beta_j(w)}^{\phi_j(w)} dx \rho(w,x) f(w,x) \qquad (41)$$

$$= (k')^2 (c + kP_N)^2 \sum_i \int_{\alpha_i}^{\omega_i} du \sum_j \int_{\beta_j(u)}^{\psi_j(u)} du \rho(u,v) f(u,v)$$

$$\times \sum_k \int_{\alpha_k}^{\omega_k} dw \sum_\ell \int dx \rho(w,x) f(w,x)$$

$$+ (k'kP_N)^2 \sum_{i,j} \left[\int_{\alpha_i}^{\omega_i} du \int_{\beta_j(u)}^{\psi_j(u)} dv \rho(u,v) f(u,v) \right]^2 \qquad (42)$$

The first term of (42) is the square of the mean value which is zero; hence,

$$\sigma_\gamma^2 = (k'kP_N)^2 \sum_{ij} \left[\int_{\alpha_i}^{\omega_i} du \int_{\beta_j(u)}^{\psi_j(u)} dv \rho(u,v) f(u,v) \right]^2 \qquad (43)$$

The double sum over the display image marks subtended by the receptive field would be tedious to evaluate. The procedure which follows will approximate the double sum by an integral. Applying the mean value theorem of integral calculus to the inner integral yields

$$\sigma_Y^2 = \left(k'kP_N\right)^2 \sum_{i,j} \left[\int_{\alpha_i}^{\omega_i} du \left[\psi_j(u) - \beta_j(u) \right] \rho(u, v_j') f(u, v_j') \right]^2 \quad (44)$$

where v_j' is a point within the interval $\psi_j(u)$, $\beta_j(u)$. Applying the same theorem to the remaining integral yields

$$\sigma_Y^2 = \left(k'kP_N\right)^2 \sum_{i,j} \left[\left(w_i - \alpha_i\right) \left[\psi_j\left(u_i'\right) - \beta_j\left(u_i'\right) \right] \rho\left(u_i', v_j'\right) f\left(u_i', v_j'\right) \right]^2 \quad (45)$$

$$= \left(k'kP_N\right)^2 \sum_i \ell_{mi}^2 \sum_j \left[w_{mj}\left(u_i'\right) \rho\left(u_i', v_j'\right) f\left(u_i', v_j'\right) \right]^2 \quad (46)$$

where $\ell_{mi} = w_i - \alpha_i$, the length of the i$^{\underline{th}}$ mark in the time dimension; $w_m(u_i) = \psi_j(u_i') - \beta_j(u_i')$, the width of a mark at u_i. The inner sum can be rewritten as:

Where $\ell_{mi} = w_i - \alpha_i$, the length of the i$^{\underline{th}}$ mark in the time dimension;

$w_m(u_i) = \psi_j(u_i') - \beta_j(u_i')$, the width of a mark at u_i.

The inner sum can be rewritten as:

$$S = \sum_j \left[w_{mj}\left(u_i'\right) \rho^2\left(u_i', v_j'\right) f^2\left(u_i', v_j'\right) \right] w_{mj}\left(u_i'\right) \quad (47)$$

which shows that the terms are a product of the factor in brackets and a width increment $w_{mj}(u_i')$. This sum can be approximated by one with a larger number of terms with a smaller width increment of constant width Δv:

$$S' = \sum_p \left[w_{mp}(u_i') \rho^2(u_i', v_p') f^2(u_i', v_p') \right] \Delta v \qquad (48)$$

Finally, this expression can be approximated by the integral

$$S'' = w_m(u_i') \int dv \left[\rho(u_i', v) f(u_i', v) \right]^2 \qquad (49)$$

where the integration is carried out over the limits of the receptive field. If the axis of the receptive field passes through the fovea, then the cone density can be approximated as a function of u_i', which for convenience can be taken as the peripheral angle, and the integration is over the width of the field w_f:

$$S'' = w_m(u_i') \rho^2(u_i, 0) \int_{-2^{-1} w_f(u_i)}^{2^{-1} w_f(u_i)} dv f^2(u_i', v) \qquad (50)$$

The weighting function is deduced from the data of Westheimer and those of Enoch et alii (see (3) and Fig. 2.7):

$$f(u,v) = \begin{cases} 0, & v < -(3/2)w_s(u) \\ -1/2, & -(3/2)w_s(u) \le v < -(1/2)w_s(u) \\ 1, & -(1/2)w_s(u) \le v \le (1/2)w_s(u) \\ -1/2, & (1/2)w_s(u) < v \le (3/2)w_s(u) \\ 0, & (3/2)w_s(u) < v \end{cases} \qquad (51)$$

Evaluating (50) with this function yields

$$S'' = (3/2)w_m\left(u_i'\right)\rho^2\left(u_i', 0\right)w_s\left(u_i'\right) \tag{52}$$

and substituting this result into (46) produces

$$\sigma_\gamma^2 = (3/2)\left(k'kP_N\right)^2 \sum_i \left[\ell_{mi}w_m\left(u_i'\right)\rho^2\left(u_i', 0\right)w_s\left(u_i'\right)\right]\ell_{mi} \tag{53}$$

The indicated sum can be approximated by one with uniform increments smaller than ℓ_{mi} giving

$$\sigma_\gamma^2 \simeq (3/2)\left(k'kP_N\right)^2 \sum_q \left[\ell_{mq}w_m\left(u_q'\right)\rho^2\left(u_q', 0\right)w_s\left(u_q'\right)\right]\Delta u \tag{54}$$

Finally, this sum is approximated by an integral:

$$\sigma_\gamma^2 \simeq (3/2)\left(k'kP_N\right)^2 \int_\alpha^\omega du\rho^2(u)w_s(u)\ell_m(u)w_m(u) \tag{55}$$

The angular dimensions of the images of display markings were derived in Section 3.3. Substituting (19) and (24) in (55) gives

$$\sigma_\gamma^2 = \frac{3hw}{2tc}\left(\frac{180 \cdot 60k'k}{\pi b \sin\gamma}P_N\right)^2 I_d \tag{56}$$

where

$$I_d = \int_\alpha^\omega du\rho^2(u)w_s(u)\sin^3(\gamma - u) \tag{57}$$

Mean Value of Response to Noise Plus Signal

The mean value of the receptive field response will be evaluated for the case in which a signal is present in frequency bin k whose trace falls within the summation region of the receptive field. Using (36) and (14) yields

$$m_{YS} = k'\left(c + kP_N\right) \sum_i \int_{\alpha_i}^{\omega_i} du\rho(u,0) \sum_{\substack{j \\ j\neq k}} \int_{\beta_j(u)}^{\psi_j(u)} dv f(u,v) \qquad (58)$$

$$+ k'\left[c + k\left(P_N + P_S\right)\right] \sum_i \int_{\alpha_i}^{\omega_i} du\rho(u,0) \int_{\beta_k(u)}^{\psi_k(u)} dv\, f(u,v)$$

$$= k'\left(c + kP_N\right) \sum_i \int_{\alpha_i}^{\omega_i} du\rho(u,0) \sum_j \int_{\beta_j(u)}^{\psi_j(u)} dv f(u,v)$$

$$+ k'kP_S \sum_i \int_{\alpha_i}^{\omega_i} du\rho(u,0)\left[\psi_j(u) - \beta_j(u)\right] \qquad (59)$$

The first term of (59) is recognized as the mean value of the response to noise alone, which is zero. The inner integral of the second term of (58) is readily evaluated since $f(u,v) = 1$ in the summation region of the receptive field, and the result appears as the second term of (59). The mean value of the response with signal is then

$$m_Y = k'kP_S \int_{\alpha}^{\omega} du\rho(u)w_m(u) \qquad (60)$$

where $w_m(u) = \psi_j(u) - \beta_j(u)$ is the width of the display mark image at u.

Substituting (24) in (60) gives

$$m_{\gamma S} = \frac{180 \cdot 60 w k' k P_S}{\pi c b \sin \gamma} I_n \qquad (61)$$

where

$$I_n = \int_{\alpha}^{\omega} du \rho(u) \sin (\gamma - u) \qquad (62)$$

The required results of this section are (61) for the mean value of the field output when the signal is present, and (56) for its variance with no signal present.

Detection Performance

In the last stage of the processing sequence depicted by Figure 3.1, it is assumed that the output of a receptive field is compared to a threshold. The performance of this stage of processing has been examined extensively in the signal processing literature. A measure of the performance is the detection parameter d, which is defined as the increase in the mean value of the stage input resulting from the signal divided by the standard deviation of the input with noise alone. For the case at hand;

$$d = m_{\gamma S}/\sigma_\gamma \qquad (63)$$

and substituting (61) and the square root of (56) in (63) gives

$$d = \sqrt{\frac{2tw}{3hc}} \quad \frac{I_n}{\sqrt{I_d}} \quad \frac{P_S}{P_N} \tag{64}$$

The first factor of (64) involves only the display parameters. The integrands of the pair of integrals defined by (62) and (57) include retinal functions and the viewing angle, and the limits are determined by both display and viewing parameters. The net effect of these parameters will be assessed by considering a special case in the sequel.

For the case at hand, the field output is a linear combination of a large number of statistically independent samples, and its distribution approaches Gaussian according to the central limit theorem. For such a case, the false alarm and detection probabilities can be expressed as

$$P_F = N(-g) \tag{65}$$

$$P_D = N(d - g) \tag{66}$$

where N( ) is the Gaussian probability distribution function for zero mean and unit variance (67)

$$g = \frac{t - m_{YN}}{\sigma_Y} = \frac{t}{\sigma_Y}, \text{ since } m_{YN} = 0 \tag{68}$$

t is the fixed threshold value.

If the detection parameter equals g, then $P_D = 0.5$. If this is regarded as the threshold of detection, then the corresponding value of the detection paremeter d_T can be employed

in (64) to determine the signal-to-noise power ratio required to achieve the detection threshold:

$$\left(\frac{P_S}{P_N}\right)_T = \frac{\sqrt{I_d}}{I_n}\sqrt{\frac{3hc}{2tw}}\, d_T \qquad (69)$$

The quantity $10 \log_{10} (P_S/P_N)_T$ is called the recognition differential (for $P_D = 0.5$).

The receptive field has a property that is very important for a functional detector. Since the mean value of its output from noise alone (m_{YN}) is zero, the value of t in (68) required to achieve a value of g required to achieve a false alarm rate as determined by (65) does not depend on the level of the noise. That is to say that no further processing (such as averaging over a larger area of the image) is required in order to determine the value of the comparison threshold. A detector with this property is said to be normalized.

The detection performance [(64) or (69)] is seen to depend on several sets of parameters and functions listed below.

1. Display parameters

   w width of display (frequency dimension)
   c number of frequency cells
   h height of display (time dimension)
   t number of time samples spanned by h

2. Viewing parameters

γ viewing angle, measured from the plane of the display

b viewing distance

3. Retinal functions

ρ density of cones in center area of receptive field

w_s width of center area of receptive field

In general, the dependence of performance on these parameters is fairly complex; however, the ratio w/c appears only once, i.e., under the radical sign in (64) or (69). This result predicts that performance improves as the raster spacing w/c in the frequency dimension increases. However, this relationship holds only when the width of the signal trace is less than the width of the receptive field. The radical sign also includes the raster spacing in the frequency dimension, h/t. However, since the limits of integration also depend on the display height h, the significance of this spacing, as well as that of other parameters will be investigated by means of a set of examples.

In the sequel, estimates of the retinal functions are applied, and the resulting equations involve only the display and viewing parameters.

3.5 Centered Image, Small Visual Angle

A special case is the one in which the trace image is centered on the retina. For this case, the limits of integration of (62) and (57) have the same magnitude, i.e., $\alpha = -\varepsilon$, and $\omega = \varepsilon$. It is further assumed that both the cone density and the width of the receptive field are even functions of the peripheral angle.

For this case (62) can be written as

$$I_n = \int_{-\varepsilon}^{\varepsilon} du\rho(u) \, (\sin \gamma \cos u - \cos \gamma \sin u) \tag{70}$$

The first and second terms of the integrand of (70) are even and odd functions of u respectively; thus, with the assumptions about the symmetry of the functions,

$$I_n = 2 \sin \gamma \int_{0}^{\varepsilon} du\rho(u) \cos u \tag{71}$$

and if ε remains below 15 degrees,

$$I_n \simeq 2I_1 \sin \gamma \tag{72}$$

where

$$I_1 = \int_{0}^{\varepsilon} du\rho(u) \tag{73}$$

For the same set of assumptions (57) can be expressed as

$$I_d \simeq 2 \sin\gamma \left(I_2 \sin^2\gamma + I_3 \cos^2\gamma \right) \tag{74}$$

where

$$I_2 = \int_0^{\varepsilon} du \rho^2(u) w_s(u) \tag{75}$$

$$I_3 = 3 \int_0^{\varepsilon} du \rho^2(u) w_s(u) u^2 \tag{76}$$

With these results, the threshold signal-to-noise ratio is

$$d = I_1 \sqrt{\frac{\sin\gamma}{I_2 \sin^2\gamma + I_3 \cos^2\gamma}} \sqrt{\frac{4tw}{3hc}} \cdot \frac{P_S}{P_N} \tag{77}$$

and the threshold signal-to-noise ratio is

$$\left(\frac{P_S}{P_N}\right)_T = d_T \sqrt{\frac{3hc}{4tw}} \sqrt{\frac{I_2 \sin^2\gamma + I_3 \cos^2\gamma}{\sin\gamma}} I_1^{-1} \tag{78}$$

The integrals designated I_1, I_2, and I_3 were evaluated using (1) for the cone density function and (3) for the width of the center area of the receptive field. Values of these integrals are listed in Table 3.1. For a given length of record or signal trace, the value of ε, the limit of integration, can be determined from (34). Corresponding values of the integrals can be determined by interpolating the tabulated values. Inspection of the table shows that I_3 is very small compared to I_2, and that the ratio of I_3 to I_2 increases with ε. Furthermore, as seen from (77) and (78), these factors are multiplied

Table 3:1

List of Values of Integrals and Ratios

ε (deg)	I_1	I_2	I_3*	$I_2 \div I_3$	$I_1 \div \sqrt{I_2}$
0.1	.610	.441			.919
0.2	1.14	.778	8.22-6		1.29
0.4	1.97	1.24	4.66-5		1.77
0.6	2.64	1.55	1.13-4		2.12
0.8	3.14	1.75	2.01-4		2.37
1.0	3.56	1.88	8.02-4		2.60
1.5	4.35	2.10	6.03-4		3.00
2.0	4.94	2.24	9.84-4		3.30
2.5	5.45	2.35	1.47-3	1595	3.56
3.0	5.86	2.44	2.11-3	1156	3.75
4.0	6.61	2.59	3.90-3	639	4.11
5.0	7.24	2.73	6.43-3	424	4.38
6.0	7.79	2.85	9.56-3	298	4.61
7.0	8.27	2.94	1.33-2	221	4.82
8.0	8.68	3.03	1.24-2	174	4.99
10.0	9.33	3.14	2.60-2	121	5.27
12.0	9.82	3.22	3.43-2	94	5.47
14.0	10.18	5.63	4.20-2	78	5.63

*Values of I_3 are given in exponential form. For example, the first entry in that column is 8.22×10^{-6}.

by $\cos^2\gamma$ and $\sin^2\gamma$ respectively, so that the value of I_3 could be significant for very small viewing angles γ and large visual angles ε. It can be readily shown that if calculation errors less than 0.1 dB are required, that the value of I_3 can be neglected if the condition

$$I_2/I_3 > 8.2/\tan^2\gamma \qquad (79)$$

is satisfied. Table 3.2 shows maximum tabulated values of the visual angle ε which satisfy that condition for various values of viewing angle γ.

Table 3:2
Maximum Values of ε Satisfying (79)

γ degrees	$8.2/\tan^2\gamma$	$\varepsilon_{max\ tab}$ degrees
5	62	3
10	114	6
15	264	10
20	1071	12

The condition (79) will be satisfied for most cases of interest because for a given record length, the visual angle decreases with the viewing angle. Given that (79) is satisfied, then

$$d = \frac{I_1}{\sqrt{I_2 \sin \gamma}} \sqrt{\frac{4tw}{3hc}} \frac{P_S}{P_N} \qquad (80)^*$$

and

$$\left(\frac{P_S}{P_N}\right)_T = d_T \sqrt{\frac{3hc}{4tw}} \frac{\sqrt{I_2 \sin \gamma}}{I_1} \qquad (81)^*$$

Values of $I_1/\sqrt{I_2}$ are listed in the last column of Table 1.

At this point, the effect of viewing distance can be qualitatively evaluated. By differentiating (34) with respect to the viewing distance, it is verified that the tangent of the viewing angle, and hence the viewing angle, varies inversely with the viewing distance. Moreover, Table 1 shows that $I_1/\sqrt{I_2}$ varies with the viewing angle, and since (80) shows that detection performance varies with this ratio, it varies inversely with viewing distance.

3.6 Example and Comparison

The performance of lofars is often specified in terms of $(P_S/N)_T$, where N is the spectral density of the noise at the input at the frequency of interest, and P_S is the signal power required to achieve a specified detection probability for a given false alarm probability. Since $P_N = NW$, where W is the filter bandwidth,

$$\left(\frac{P_S}{N}\right)_T = W\left(\frac{P_S}{P_N}\right)_T \qquad (82)$$

*The procedures for utilizing (80) or (81) are discussed in the last paragraph of this report, which begins on page 56.

where $(P_S/P_N)_T$ is given by either (81), (78), or (69).

The variation of the recognition differential 10 $\log_{10}$ of $(P_S/N)_T$ as a function of the record length in time units is shown by Figure 3.5 for several values of the viewing angle γ. The display parameters are those of one of the operational lofar equipments, and the viewing distance is assumed to be 18 inches. The curves show (1) that there is a declining rate of improvement with increasing record length, and (2) that a significant advantage can be obtained by decreasing the viewing angle γ. This effect is utilized by sonar operators and has been verified by detection threshold measurements.[7]

Detection threshold levels of lofar equipment have been measured by means of psychophysical experiments conducted in a laboratory. Both signals and noise are applied to the input, and the signal level required for a designated probability of detection is determined. The dashed curve of Figure 3.6 connects data obtained in one series of experiments. In these experiments, the operators are not constrained to a particular viewing distance and angle, nor are they limited to a single look at the record. Thus these data can not be employed in a direct comparison with the predictions obtained with the method developed in the report. Nonetheless, the prediction for a viewing angle of 90° at a distance of 18" is shown on Figure 3.6. These parameter values are considered nominal for the type of experiment that was conducted.

---

[7]This effect is also mentioned in B. J. Pernick and C. Bartolotta, "Signal Enhancement in Acoustic-Spectral Displays by Optical-Spatial Filtering," *U.S. Navy Journal of Underwater Acoustics*, Vol. 18, No. 1, Jan. 1968, p. 122, footnote 4.

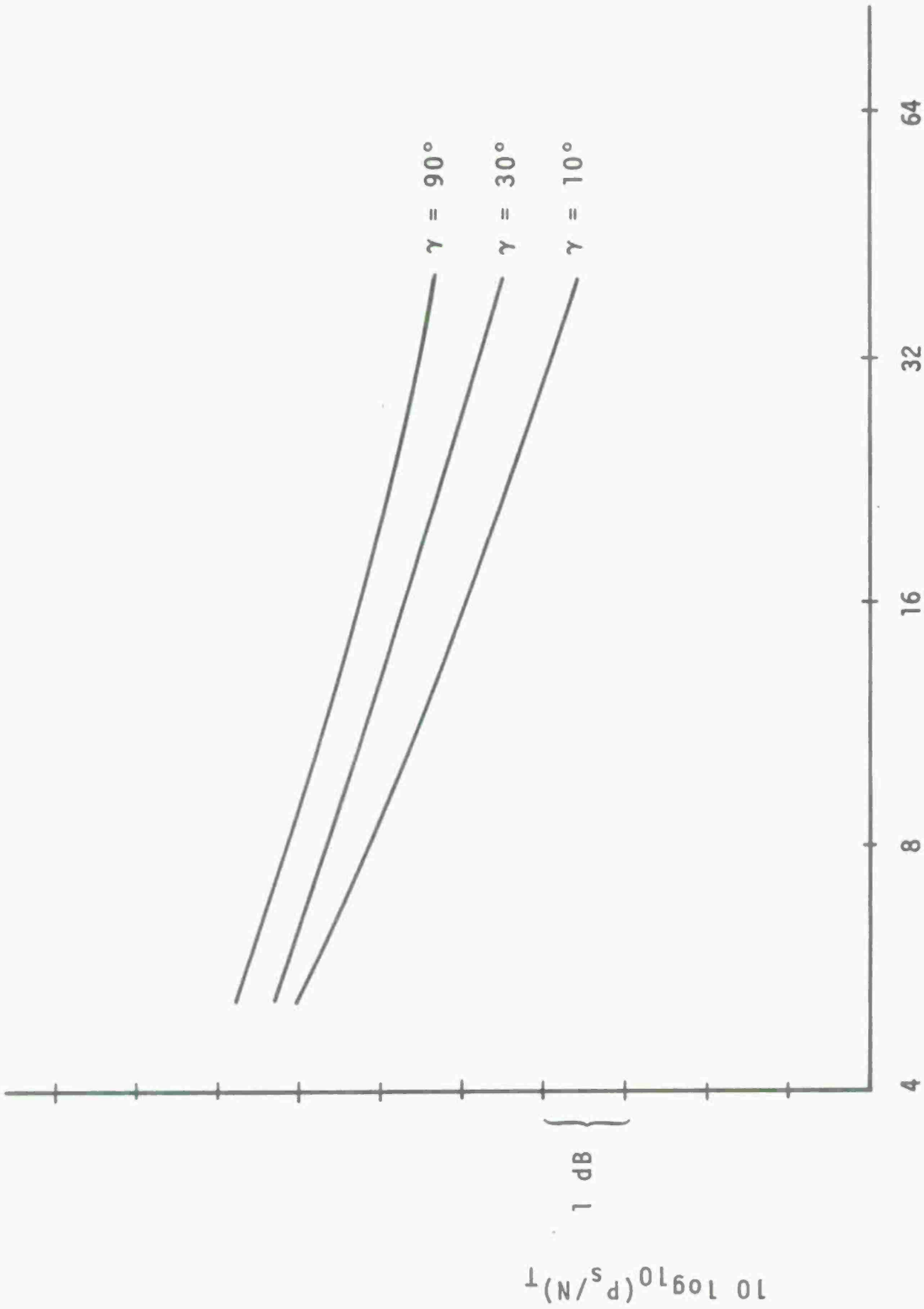

FIGURE 3.5 Effect of Record Length and Viewing Angle.

The lofar process is often modeled as an ideal detector consisting of a filter, squarer, uniform averager, and threshold detector.* The performance prediction based on this analog is also shown on Figure 3.6. This prediction is, at best, 4 dB overly optimistic, and the error increases with record length.

Given reasonable assumptions about viewing parameters, the results obtained in this report appear well suited for predicting the performance of lofars whose raster parameters have been specified.

The performance prediction equations, e.g., (80) show a factor t/h under the radical sign. This quantity is the reciprocal of the length of a display mark in the time dimension. Thus it appears that decreasing this length, i.e., compressing the display in the time dimension would improve performance. However, the visual angle ε varies with h, as can be determined from (34), and the quantity $I_1/\sqrt{I_2}$ increases with ε, and it is not immediately obvious how performance varies with h. The results of calculations, shown in Figure 3.7, indicate that a modest improvement of performance can be achieved by decreasing h. The improvement is more significant at higher viewing angles and longer record lengths. Laboratory experiments with the same degree of compression (25) show an average improvement of 0.4 dB for a ten-minute record.

It is concluded that (80) and (81) provide a convenient means for obtaining the detection parameter and the threshold signal-to-noise ratio respectively. Table 3.1 gives values

*This model is discussed in C. N. Pryor, op. cit., pp. 2-13.

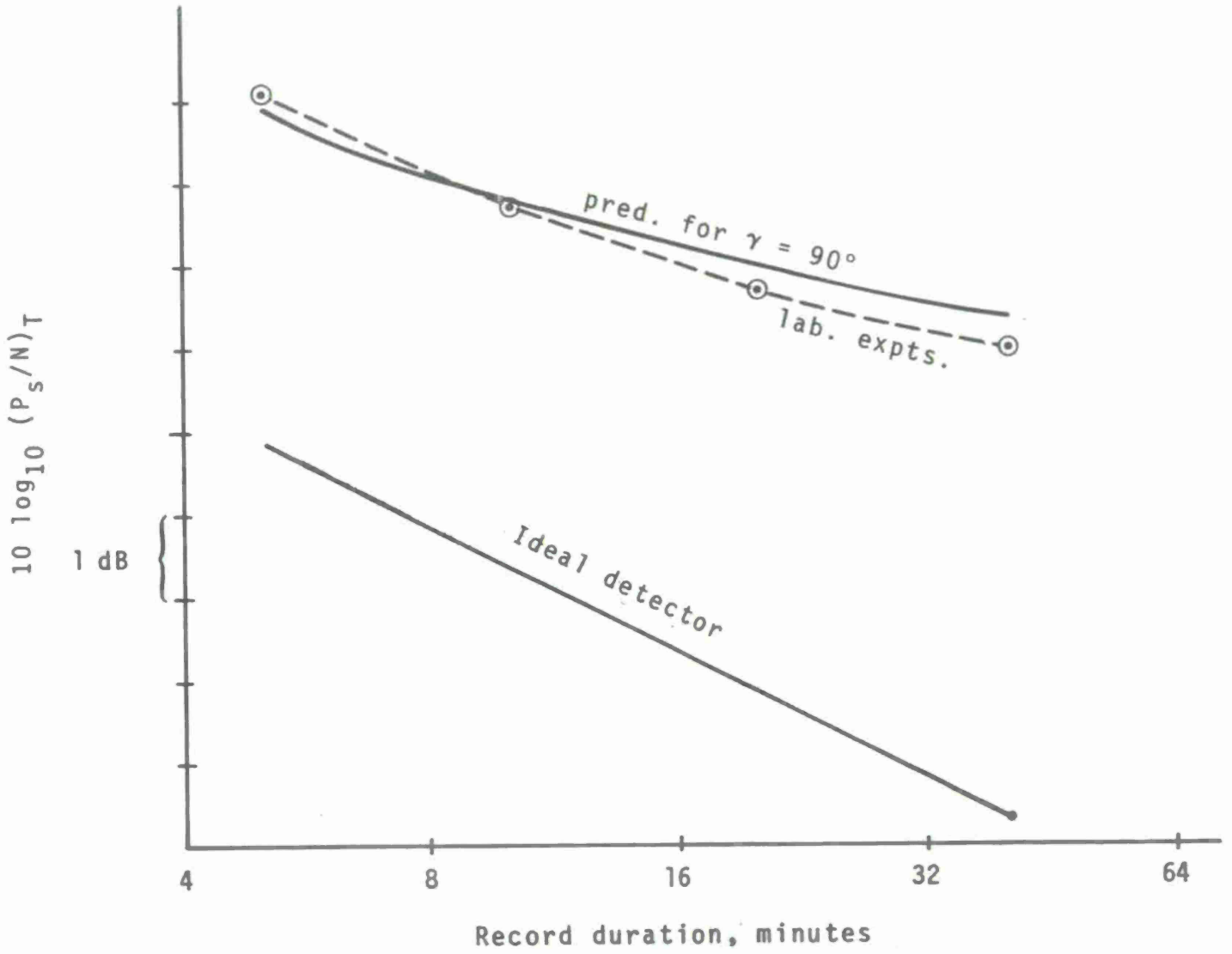

FIGURE 3.6 Comparison of Predictions and Experimental Data.

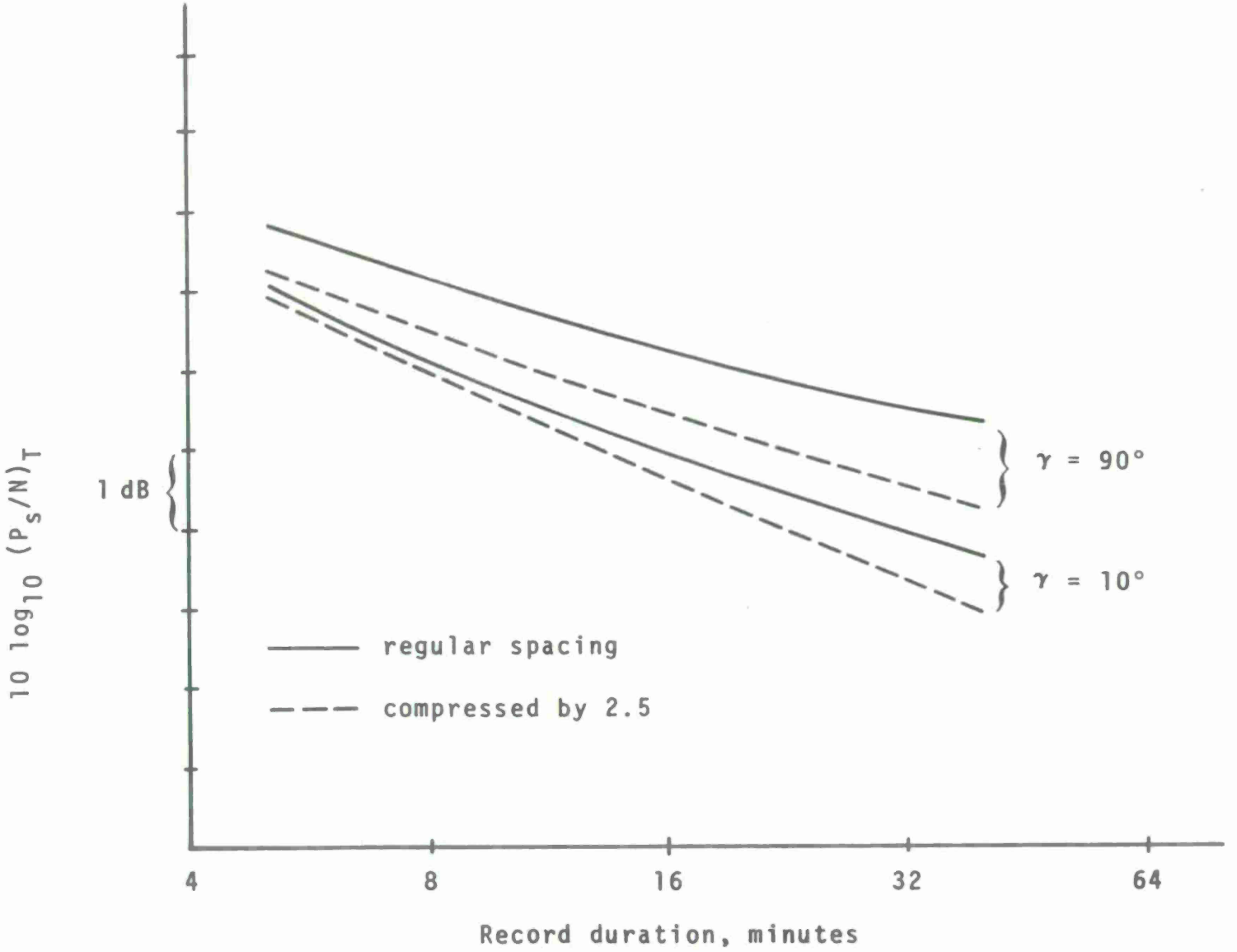

FIGURE 3.7 Effect of Compression in the Time Dimension.

of $I_1 \div \sqrt{I_2}$ for various values of ε. The value of ε for a given trace length and viewing parameters can be determined from (34). To obtain the probability of detection, the detection parameter is substituted in (66); the value of g required in (66) is obtained by solving (65) for a specified false alarm probability. If the threshold ratio is desired in terms of the noise spectral density (vice its power) then (83) should be employed in conjunction with (82). Definitions and units of the display and viewing parameters are listed below for convenience.

w Width of record (frequency dimension), inches

c Number of frequency cells spanned by width of record

h Length of record (time dimension), inches

t Number of time samples spanned by length of record

For paper recorders

$$\frac{h}{t} = \frac{s}{c}$$

s Speed at which paper advances, inches/minute

r Stylus sweep frequency, number/minute

γ Angle between display surface and line of sight to signal trace center--See Fig. 3.3.

BIBLIOGRAPHY

1. Atkinson, J., "The Effect of Size, Retinal Locus, and Orientation on the Visibility of a Single Afterimage," *Perception and Psychophysics*, 12:2B, pp. 213-216, (1972).

2. Barlow, H. B., "Retinal Noise and Absolute Threshold," *J. Acoust. Soc. Amer.*, 46:8, pp. 634-639, (August 1956).

3. Barlow, H. B., Fitzhugh, R., Kuffler, S. W., "Change of Organization in the Receptive Fields in the Cat's Retina During Dark Adaptation," *J. Physiol.*, 137, pp. 338-354 (1957).

4. Barlow, H. B., Narasimhan, R., Rosenfeld, A., "Visual Pattern Analysis in Machines and Animals," *Science*, 177:4049, pp. 567-575 (August 18, 1972).

5. Beck, J., Ambler, B., "The Effects of Concentrated and Distributed Attention on Peripheral Acuity," *Perception and Psychophysics*, 14:2, pp. 225-230 (1973).

6. Berger, C., "The Problem of Peripheral Visual Acuity," *Amer. J. of Psychology*, 61:4, pp. 603-604.

7. Blackwell, H. R., "Neural Theories of Simple Visual Discriminations," *J. Optical Soc. Amer.*, 53:1, pp. 129-160 (January 1963).

8. Brindley, G. S., "Afterimages," *Scientific American*, pp. 85-90 (October 1963).

9. Cornsweet, T. N., *Visual Perception*, Academic Press: New York (1970).

10. Cornsweet, T. N., Pinsker, H. M., "Luminance Discrimination of Brief Flashes Under Various Conditions of Adaptation," *J. Physiology*, London, 176, pp. 294-310.

11. Enoch, J. M., Hope, G. M., "Interferometer Resolution Determinations in the Fovea and Parafovea," *Documenta Opth.*, 34, pp. 143-156 (1973).

12. Enoch, J. M., Sunga, R. N., Bachmann, E., "Static Perimetric Technique Believed to Test Receptive Field Properties I Extension of Westheimer's Experiments on Spatial Interaction," *Amer. J. Ophthalmology*, 70:1, pp. 113-126 (July 1970).

BIBLIOGRAPHY (cont'd)

13. Enoch, J. M. Sunga, R. N., Bachmann, E., "Static Perimetric Technique Believed to Test Receptive Field Properties II Adaption of the Method to the Quantitative Perimeter," *Amer. J. Ophthalmology*, No. 1, pp. 126-137 (July 1970).

14. Fankhauser, F., Enoch, J. M., "The Effects of Blur on Perimetric Thresholds," *Arch. of Opthalmology*, 68:2, pp. 240-51 (1962).

15. Ferree, C.E., Rand, G., Hardy, C., "Refraction for the Peripheral Field of Vision," *Arch. of Opthalmology*, 5, pp. 719-731 (1931).

16. Gelade, G.A., Poole, C. L., Beurle, R. L., "The Pooling of Excitation in Threshold Bar Stimuli," *Vision Res.*, 14, pp. 317-327.

17. Glezer, V. D., "The Receptive Field of the Retina," *Vision Res.*, 5, pp. 497-525, Pergamon Press (1965).

18. Green, D. G., "Regional Variations in the Visual Acuity for Interference Fringes on the Retina," *J. Physiology*, 207, pp. 351-356 (1970).

19. Hopkin, V. D., "A Selective Review of Peripheral Vision," *Brit. Air Ministry RPRC 1078.*

20. Hubel, D. H., Wiesel, T. N., "Receptive Fields of Single Neurones in the Cat's Striate Cortex," *J. Physiology*, 148, pp. 574-591 (1959).

21. Hubel, D. H., Wiesel, T. N., "Receptive Fields, Binocular Interaction and Functional Architecture in the Cat's Visual Cortex," *J. Physiology*, 160, pp. 106-154 (1962).

22. Hubel, D. H., Wiesel, T. N., "Shape and Arrangement of Columns in Cat's Striate Cortex," *J. Physiology*, 165, pp. 559-568 (1963).

23. Ikeda, H., Wright, M. J., "Differential Effects of Refractive Errors and Receptive Field Organization of Central and Peripheral Ganglion Cells," *Vision Res.*, 12, pp. 1465-1476, Pergamon Press (1972).

24. Ikeda, H., Wright, M. J., "Functional Organization of the Periphey Effect in Retinal Ganglion Cells," *Vision Res.*, pp. 1857-1879, Pergamon Press (1972).

BIBLIOGRAPHY (cont'd)

25. Kelly, D. H., "Effects of the Cone-Cell Distribution on Pattern-Detection Experiments," *J. Optical Soc. Amer.*, 64:11, pp. 1523-1525 (Nov. 1974).

26. Kerr, J. L., "Visual Resolution in the Periphey" *Perception and Psychophysics*, 9, pp. 375-378 (1971).

27. Kinchla, R. A., "Detecting Target Elements in Multi-element Arrays: A Confusability Model" *Perception and Psychophysics*, 15:1, pp. 149-158 (1974).

28. Lamar, E. S., Hecht, S., Hendley, C. D., Sklar, S., "Size, Shape, and Contrast in Detection of Targets by Daylight Vision. II Frequency of Seeing and the Quantan Theory of Cone Vision," *J. Optical Soc. Amer.*, 38:9, pp. 741-755 (Sept. 1948).

29. Leibowitz, H. W., Johnson, C. A., Isabelle, E., "Peripheral Motion Detection and Refractive Error," *Science*, 177:29, pp. 1207-1208 (Sept. 1972).

30. Low, F. N., "The Peripheral Visual Acuity of 100 Subjects," *Am. J. Physiol.*, 140:83-88 (1943).

31. Low, F. N., "Peripheral Vision Acuity," *AMA Arch. of Opthal.*, 45, pp. 80-99 (1951).

32. Mackworth, N. H., "Visual Noise Causes Tunnel Vision," Internal Memorandum, Harvard University, April, 1965.

33. McAndrew, T. V., "A Computer-Simulated Model of Visual Signal Processing," NUSC Technical Report No. 4323, 30 May 1972.

34. Mandelbaum, J., Sloan, L. L., "Peripheral Visual Acuity - with Special Reference to Scotopic Illumination," *Am. J. Opthal.*, 30:581-88 (1947).

35. Menzer, G. W., Thurmond, J. B., "Form Identification in Peripheral Vision Perception and Psychophysics" 8(4), pp. 205-209 (1970).

36. Merchant, J., "Sampling Theory for the Human Visual Sense," *J. Opt. Soc. Am.*, 55:10, pp. 1291-1295 (Oct. 1965).

BIBLIOGRAPHY (cont'd)

37. Ogle, K. N., "Peripheral Contrast Thresholds and Blurring of the Retinal Image for a Point Light Source," *J. Opt. Soc. Am.*, 51:11, pp. 1265-1268 (Nov. 1961).

38. Pirenne, M. H., "Quantum Physics of Vision: Theoretical Discussion in Progress in Biophysics, Pergamon Press, London, 2, pp. 193-223 (1951).

39. Randall, H. G., Brown, D. J., Sloan, L. L., "Peripheral Visual Acuity," *Arch. Opthal*, 75, pp. 500-501 (April 1966).

40. Ratliff, F., Hartline, H. K., Miller, W. A., "Spatial and Temporal Aspects of Retinal Inhibition Interaction," *J. Opt. Soc. Am.*, 53:1, pp. 110-120 (Jan. 1963).

41. Rondchi, L, Salvi, G., "Performance Decrement, Under Prolonged Testing, Across the Visual Field," *Opthal, Res. S.*, pp. 113-120 (1973).

42. Sloan, L. L., "Area and Luminance of Test Object as Variables in Examination of the Visual Field by Projection Perimetry," *Vision Research*, 1, pp. 121-138 (1961).

43. Stein, K. J., "Optical Device Studies Flight Displays," *Av. Week & Space Tech.*, pp. 52-55 (Jan. 28, 1974).

44. Sunga, R. N., Enoch, J. M., "A Static Perimetric Technique Believed to Test Receptive Field Properties III Clinical Trials," *Am. Jour. Opthalmology*, 70:2, pp. 244-272 (Aug. 1970).

45. Taylor, J. H., "Contrast Thresholds as a Function of Retinal Position and Target Size for the Light-Adapted Eye," *Scripps Institute of Oceanography*, Ref. 61-10, (March 1961).

46. Uttal,W. R., Bunnell, L. M., Corwin, "On the Detectability of Straight Lines in Visual Noise: An Extension of French's Paradigm into the Millisecond Domain," *Perceptor & Psychophysis*, 8(6), pp. 385-388 (1970).

BIBLIOGRAPHY (cont'd)

47. Vallerie, L. L., Link, J. M., "Visual Detection Probability of 'Sonar' Targets as a Function of Retinal Position and Brightness Contrast," *Human Factors*, 10(4), pp. 403-411 (1968).

48. von Wright, J. M., Mikkonen, V., "The Influence of Alcohol on the Detection of Light Signals in Different Parts of the Visual Field," *Scand. J. Physiol*, II, 167-175 (1970).

49. Weale, R. A., "Problems of Peripheral Vision," *Brit. J. Opthal.*, 40, pp. 392-415 (1956).

50. Westheimer, G., "Spatial Interaction in Human Cone Vision," *Journal of Physiology*, 195, p. 97 (1968).

51. Westheimer, G., Campbell, F. W., "Light Distribution in the Image Formed by the Living Human Eye," *J. Opt. Soc. Am.*, 52:9, pp. 1040-1045 (Sept. 1962).